THE SYNTHESIS AND CHARACTERISATION OF LEAD-FREE PIEZOELECTRIC CERAMICS

by

William Michael Roberts

A thesis submitted to

The University of Birmingham

for the degree of

Master of Research in Science and Engineering of Materials

Department of Metallurgy and Materials

School of Engineering

University of Birmingham

October 2011

Abstract

With a growing awareness of the environmental and health hazards of lead, there has been renewed interest in developing lead-free alternatives to lead zirconate titanate (PZT), which currently dominates the market for piezoelectric materials. Some of the most promising lead-free piezoelectric materials are those based on potassium sodium niobate (KNN). This project involved the fabrication and characterisation of lithium-doped KNN ceramic, which has been reported to show excellent piezoelectric properties. Samples containing 0-9 mol% Li were synthesised by a conventional mixed oxide method, before their key functional properties were analysed. The addition of lithium was found to promote grain growth within the microstructure, resulting in a denser ceramic. A phase transformation from the orthorhombic to tetragonal crystal structure was also identified. Optimum piezoelectric properties were observed in KNN samples containing 7 mol% Li (k_p=0.33, k_t=0.37, d_{33}=126 pC/N). Further optimisation of the fabrication route and continued investigation into the most effective dopants could potentially bring KNN on a par with many commercial lead-based ceramics.

Acknowledgments

I would like to thank my supervisor Tim Button for his guidance and supervision throughout this research project. Gang Liu and Carl Meggs for their help with experimental procedures and lastly, the Department of Metallurgy and Materials for the studentship which helped support me financially.

Table of Contents

1. INTRODUCTION 1
1.1 Piezoelectricity 1
1.2 Piezoelectric Materials and Applications 2
1.3 Lead-free alternatives - current research 6
1.3.1 Tungsten-Bronze structures 8
1.3.2 Bismuth layered structures 10
1.3.3 Lead-free perovskites 10
1.4 Project Aims and Objectives 18
2. EXPERIMENTAL APPROACH 20
2.1 Fabrication Procedure 20
2.2 Electrical Characterisation 26
3. RESULTS AND DISCUSSION 32
3.1 Precursor analysis 32
3.1.1 X-ray diffraction 32
3.1.2 SEM micrographs 34
3.2 Calcined powder analysis 35
3.2.1 X-ray diffraction 35
3.2.2 SEM micrographs 36
3.2.3 Particle size analysis 37
3.3 Sintered ceramic analysis 38
3.3.1 X-ray diffraction. 38
3.3.2 Density 39
3.3.3 Sintered microstructures 41
3.4 Functional Characterisation 42
3.4.1 Piezoelectric coefficient (d_{33}) 42
3.4.2 Electromechanical coupling coefficients (k_p, k_t) 44
3.4.3 Relative permittivity (ε_r) 45
4. CONCLUSION 50
5. FURTHER WORK 52
6. REFERENCES 54

1. INTRODUCTION

This project involves fabricating and characterising lead-free piezoelectric ceramic. This past decade has seen much interest in the potential development of a non-lead alternative to the lead-based electroceramics that currently dominate the market for piezoelectric devices. The environmental and health hazards of lead are well documented, and in other industries much has been done to minimise its use, but currently a viable lead-free piezoelectric material has yet to be found, and the increasing demand for high-performance piezoelectric materials means that lead use is a growing concern. This section gives an introduction to piezoelectricity and the focus of current research on the subject.

1.1 Piezoelectricity

Piezoelectricity is the ability of some materials, commonly ceramics, to produce an electrical potential when placed under a mechanical stress. Similar to the pyroelectric effect, where a material generates an electric potential in response to a temperature change, it was first researched in the late-18th century, where drawing on the knowledge of the pyroelectric effect, a relationship between mechanical stress and electric charge was observed. However, it was not until 1880 that brothers Jacques and Pierre Curie demonstrated what is now known as the piezoelectric effect when they noticed an unusual characteristic in some crystalline materials, where by the crystals became electrically polarised in response to an applied force. The voltage generated was in proportion to the applied force and would either be negative or positive depending on if the material was in compression or tension. The effect was later found to be reversible; if a voltage-generating crystal was exposed to an electric field, it would distort, either expanding or contracting according to the polarity of the field. These phenomena later became known as the piezoelectric effect and inverse piezoelectric effect respectively, after the Greek word

piezein, meaning to press. Before the piezoelectric effect could be harnessed, a greater understanding of the crystal structures that exhibited piezoelectricity was required. By the turn of the 20th century, of the 32 classes of natural crystalline materials, 20 of them were identified as being capable of piezoelectricity. All 20 of these crystals are non-centro symmetric. For a material to demonstrate an anisotropic effect such as piezoelectricity, it is necessary that the crystal structure has no centre of symmetry.

The piezoelectric effect itself can be closely related to the occurrence of electric dipole moments within the material. The positive and negative electrical charges present in a piezoelectric crystal are symmetrically arranged, cancelling one another out and rendering the crystal as a whole electrically neutral. Electric dipole moments are the vector lines separating the opposite charges. The dipoles form domains; regions where neighbouring dipoles have the same alignment. A crystal consists of multiple interlocking initially randomly oriented domains. In order to create a net polarisation across the ceramic sample an alignment of the domains through a process known as poling is required. This involves applying an electric field to the ceramic that forces the domains to align parallel to the field lines produced. When the crystal is put under stress, the symmetry is partially lost and the charges no longer cancel each other out, with net positive and negative charges appearing on opposite crystal faces.

1.2 Piezoelectric Materials and Applications

Piezoelectricity was first found to exist in naturally-occurring crystals such as Quartz and Tourmaline, but today exists in many man-made crystals and ceramics. Ceramics that could exhibit the piezoelectric effect were not discovered for nearly 40 years after the first practical applications for piezoelectricity had been developed. Until then, natural crystals such as Quartz were being used in piezoelectric devices. One of the first applications to

utilise piezoelectric devices was sonar. Thin Quartz crystals were used as transducers in an ultrasonic submarine detector during World War I. The success of this project led to increased interest in piezoelectric devices and new applications for such devices were explored.

During World War II, a new class of materials called ferroelectrics were discovered. This would revolutionise the piezoelectric industry as it allowed piezoelectric ceramics to be fabricated for the first time. Ferroelectrics possess a spontaneous electric polarisation that can be reversed by the application of an external electric field. This allowed polycrystalline ceramics comprising of a mass of sintered single crystals to be fabricated. Normally this would have resulted in a ceramic with randomly oriented domains and therefore unable to exhibit piezoelectric properties. But the spontaneous electric polarisation that ferroelectrics possess means they can be poled to achieve domain alignment, so the ceramic is effectively behaving as a single crystal would, with one direction of polarisation.

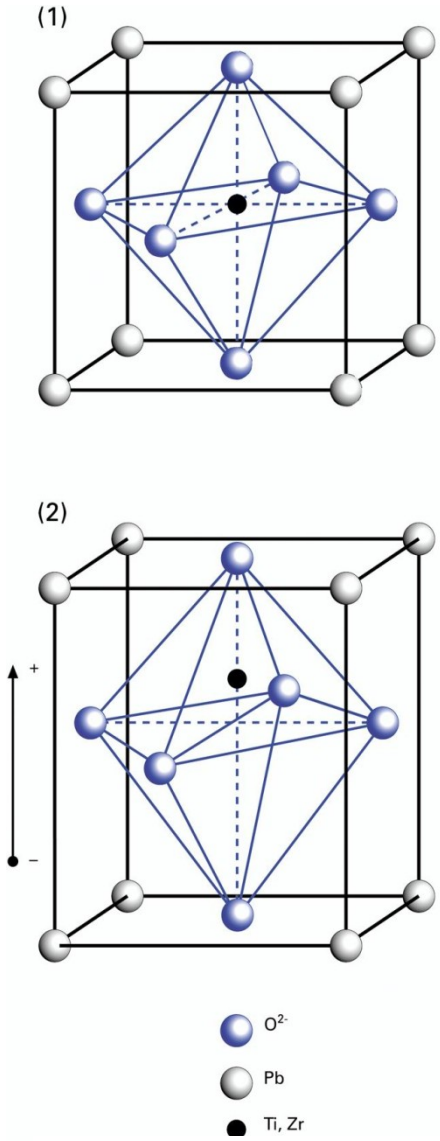

Figure 1.1

(1)PZT unit cell in cubic state above the Curie temperature

(2) Distorted tetragonal unit cell below the Curie temperature (http://www.physikinstrumente.com/en/products/primages.php?sortnr=400600.00)

This granted far more scope in the development of piezoelectric materials, and it was not long before the first piezoceramics were fabricated, possessing far superior piezoelectric properties to the natural crystal that had been used up until that point. Ferroelectric

ceramics, in particular those with a perovskite structure, became particularly widely used. These polycrystalline materials comprised of many crystallites that shared the same crystal structures as calcium titanate, known as the perovskite structure. This means that they exist in two crystallographic forms; above the Curie temperature, a simple cubic structure with no dipole moment, whilst below the Curie temperature a transformation occurs into the tetragonal structure, where the dipole moments form domains (Fig 1.1). It's in this state that the ceramic can exhibit piezoelectric properties once the domains have been aligned.

Although barium titanate was the first ferroelectric ceramic to be used for its piezoelectric properties, it was soon surpassed by the perovskite lead zirconate titanate ($Pb(Zr,Ti)O_3$, PZT), a material with exceptional piezoelectric properties and a high dielectric constant

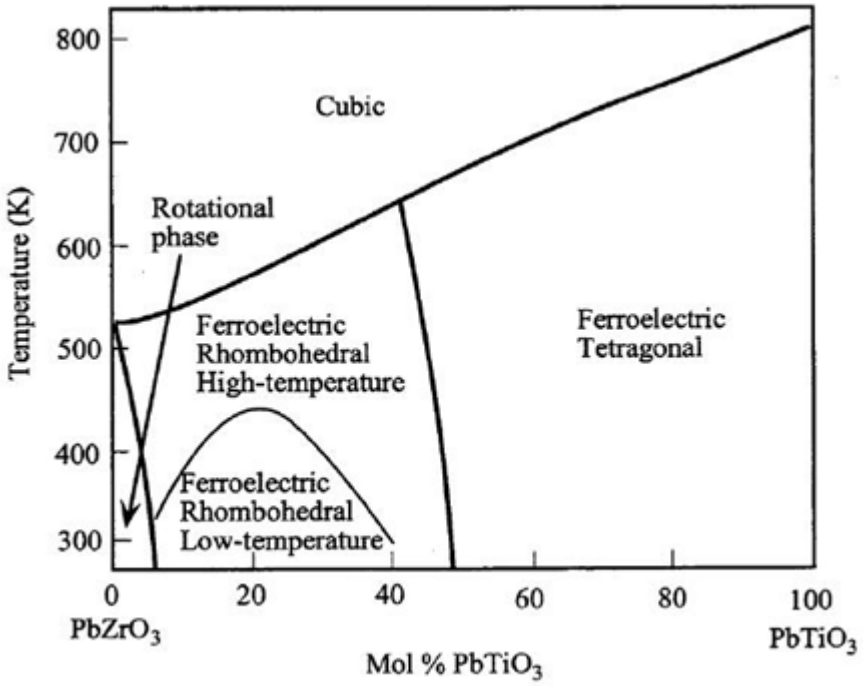

Figure 1.2 PZT phase diagram. MPB at ~48 mol% $PbTiO_3$, reproduced from http://www.doitpoms.ac.uk/tlplib/piezoelectrics/pzt.php

which dominates the market for piezoceramic components currently. PZT is typically fabricated by the mixed oxide route from starting powders, and compositionally, most PZT ceramics lie near a morphotropic phase boundary (MPB) separating tetragonal and rhombohedral phases. In this region the important functional properties such as the

piezoelectric and electromechanical coupling coefficients and permittivity peak (Fig 1.2). To further its range of potential applications, it can be doped with certain donor and acceptor dopants to allow for the manufacture of soft and hard PZT's respectively. This greatly increases the versatility of PZT, with 'soft' ceramic exhibiting enhanced piezoelectric constants and coupling factors but being relatively easy to depolarise, whilst 'hard' ceramics have comparatively poor piezoelectric properties but have a larger coercive field, are more difficult to depolarise and have very low dielectric losses, making them more practical for certain applications.

Many of the key applications of piezoelectric materials involve utilising them as sensors or actuators. With the development of high-performance ferroelectric ceramics came the ability to use these materials in a wide range of sensing applications. The principles of the sensor involve exploiting the direct piezoelectric effect to detect vibrations or stress of objects by outputting an electrical signal in response to an applied force. This fundamental sensing technique can be adapted for use in applications such as microphones, where acoustical pressure is turned into a voltage, and pressure sensors in mobile phones. Actuators work on the same basic principle, but use the inverse piezoelectric effect. When subjected to an electric field, a distortion of the piezoelectric material results. With very high electrical fields often only corresponding to a change in dimensions in the range of micrometers, it is possible for piezoelectric actuators to position objects with extreme accuracy. Advanced imaging techniques such as atomic force microscopy use piezoelectricity to carefully control the distance between the sensing needle and the probe.

Piezoelectric transducers use the piezoelectric material in dual capacity. Electrical pulses are converted to mechanical vibrations which travel outward, returned vibrations are then converted back into an electric signal. Transducers that operate at extremely high

frequencies, above 20,000 hertz, are known as ultrasonic transducers. At these frequencies it is possible to accurately map objects in high resolution, making them widely used for biomedical imaging, non-destructive testing and underwater sonar. PZT has many of the desirable piezoelectric properties for use in these high frequency ultrasonic transducers, including a large electromechanical coupling coefficient and large dielectric constant. As such, PZT has become the dominant material in the ultrasonic transducer industry in the past 40 years.

1.3 Lead-free alternatives - current research

As discussed, PZT is currently the most widely used piezoelectric material for numerous electronic devices utilising actuators, sensors and transducers. Recently, however, there has been a growing awareness of the environmental and health hazards of lead. A major drawback of PZT is that it contains more than 60 wt% lead; a toxic heavy material. With the increasing use of PZT, more and more lead oxide and lead zirconate titanate is being released into the environment during the materials' life-cycle. This can occur during calcination and sintering, where excess PbO from the starting oxides is evaporated. Waste material is also produced during machining, and after usage there is the issue of recycling and waste disposal. Recycling and disposing of devices containing lead-based piezoelectric materials is now a great concern, especially when considering that these materials are now used extensively in large consumer products such as cars, sound equipment and medical devices. In 2003 the EU included PZT in its legislation, advising it be substituted as a hazardous material by safer materials. More recent EU legislation, namely the Restriction of Hazardous Substances Directive that came into effect in 2006, restricts the use of lead in the manufacture of various types of electrical equipment. This legislation has already been

largely responsible for lead-free solder being widely adopted, and similar strides are expected to be made in the piezoelectric industry, with a renewed interest in the development of environmentally friendlier lead-free piezoelectric materials over the last 10 years. Aside from the environmental aspect, other motivations for researching these new materials include the need for piezoelectric devices that are suitable for high temperature operations, and the prospect of new piezoelectric applications in biological settings, given the health concerns associated with lead. There is a growing interest in sensors and actuators that can be implanted directly into living tissue. The challenge for researchers is to develop a lead-free piezoelectric that appeals to a wide array of applications, whilst achieving comparable piezoelectric properties to PZT.

Unfortunately, among existing lead-free piezoelectric materials, many exhibit relatively weak piezoelectricity. An example of this is $LiNbO_3$, which was first discovered to be ferroelectric in 1949. Its combination of piezoelectric and electro-optic properties makes it useful for electro-optic applications and a frequent replacement for quartz in a number of applications (1), but for more demanding piezoelectric applications it is scarcely used. Current research is mostly focused on three groups of lead-free piezoelectric materials, based on perovskite, tungsten-bronze and bismuth layered structures. It is not limited to these however, with renewed interest in some of the earliest lead-free piezoelectric materials such as barium titanate.

Barium titanate ($BaTiO_3$) has long been seen as a potential lead-free alternative to PZT but has been limited in the applications it can be used for by its low-phase transition temperature, making it suitable only for low temperature and room temperature applications. Its widespread use has been further hindered by high fabrication costs. It was initially used for microphones and certain transducer applications before being largely

replaced by PZT. The recent legislation however, has led to renewed interest in this ceramic, where efforts to fabricate high performance lead-free $BaTiO_3$ have been investigated (2). Most of the work currently ongoing is centred on improving the density of the material by using modern fabrication techniques. High density barium titanate has been shown to have greatly improved piezoelectric properties over barium titanate fabricated through classical means (3). This has been achieved by fabricating the material through a hydrothermal method, where a particle size of 100 nm is achieved prior to a two-step sintering stage. By this method, final densities of 98.3% theoretical value have been obtained, with properties comparable to conventional PZT. Doubts still exist, however, around whether this complex fabrication technique is feasible on a much larger scale.

1.3.1 Tungsten-Bronze structures

Piezoelectric ceramics based on the tungsten-bronze crystal structure were the first ferroelectric material discovered that did not crystallise in the perovskite structure. Tungsten-bronze is the structure of lead metaniobate ($PbNb_2O_6$, PN). This ceramic is considered to be an excellent ferroelectric for applications in high temperature conditions due to its high Curie temperature (~570 °C). It has three crystal structures; a low-temperature rhombohedral form, a high temperature tetragonal form and a metastable orthorhombic structure that is achieved through rapid cooling through the Curie temperature. This middle phase is the only phase that has ferroelectric and piezoelectric properties. A drawback that has stopped it from becoming as widely used as PZT is the difficulty in achieving high-density samples with fine-grained microstructures, due to rapid grain growth that occurs during the phase transformation from the low temperature to high temperature form (4). Furthermore, its piezoelectric constant, d_{33} is somewhat lower than that of PZT.

Whilst this material has struggled to replace PZT, lead-free alternatives based on the tungsten-bronze structure have shown recent promise (5). There are a number of lead-free compounds in the tungsten-bronze family that exhibit the piezoelectric effect. Among the most attractive are the systems that have a potential morphotropic phase boundary (MPB), a compositional region where functional properties may peak. $(Sr_{1-x}Ba_x)_2NaNb_5O_{15}$ (SBNN) is one such compound that exhibits a MPB at a certain composition. Jiang et al. found that single crystals of the compound with compositions approaching the MPB had superior piezoelectric and dielectric properties to many perovskite single crystals (6). Its high ferroelectric phase transition temperature means its properties are less temperature sensitive than other lead-free candidate materials such as $BaTiO_3$. Sintered polycrystalline variants though have proven less successful. They have been found to be limited to lower frequency applications, because of the large losses at higher frequencies from the scattering of ultrasound at grain boundaries (7). Also, the tungsten-bronze structure has been noted to have inferior crystallographic symmetry to the perovskite structure, resulting in difficulties with the control of domains. Complex grain orientation techniques are usually required to bring the piezoelectric properties on a par with other lead-free piezoceramics (5).

1.3.2 Bismuth layered structures

First researched in 1985 by Shebanov et al (8), complex bismuth oxides with layered structures are a group of ferroelectrics characterised by their high Curie temperature (up to 980 °C), strong electromechanical coupling factors and low aging rate. In theory, this makes them suitable for use as piezoelectric materials operated at high temperatures and high frequencies. They are built up by the regular intergrowth of $(Bi_2O_2)^{2+}$ layers on perovskite-like slabs (Fig 1.3). With this layered structure, the compositions exhibit very high anisotropy of properties.

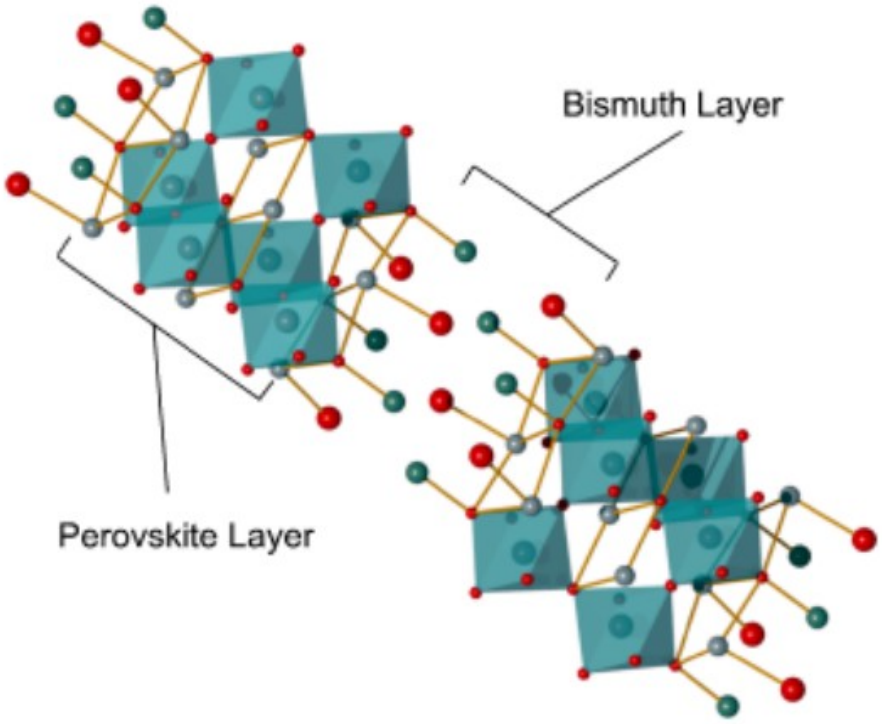

Figure 1.3 Bismuth layered structure. Perovskite layers separated by Bi_2O_2 layers, reproduced from Rödel et al (29).

1.3.3 Lead-free perovskites

Most research is currently focused on the perovskite group of lead-free piezoelectrics. This group includes Bi-based materials such as bismuth sodium titanate (BNT), a promising lead-free candidate material first discovered in 1961 (9). BNT features a large remnant

polarisation and high coercive field with a relatively high Curie temperature (320 °C). Like many lead-free perovskites, its main drawback is its high conductivity, giving rise to ineffective poling. BNT also requires a high sintering temperature (>1200 °C) to obtain a dense body. Pure BNT is no longer seen as a realistic alternative to PZT, but recent research suggests it responds well to various dopants (10). It has been reported that modified BNT-based compositions obtained by conventional ceramic processing have shown improved properties and easier treatment in the poling process. One of the more promising compositions is a BNT-$BaTiO_3$ binary system, which shows the existence of a rhombohedral-tetragonal morphotropic phase boundary. BNT-based binary systems with a MPB composition have shown improved piezoelectric and pyroelectric properties compared to unmodified BNT, with reports of the d_{33} value more than doubling (11). A ternary system investigated by Chan et al. has been found to have comparable properties to PZT and is seen as a potential candidate for use in the fabrication of ultrasonic wirebonding transducers (12). However for BNT systems, the curved nature of the MPB leads to poor temperature stability and the presence of a depolarisation temperature below the Curie temperature limits its use in high temperature applications.

Table 1.1 Functional properties of some selected piezoelectric ceramics

Material	ε_r	d_{33}	k_p	k_t	k_{33}	T_C	References
PZT "Soft" Pz27	1800	425	0.59	0.47	0.7	350	(13)
PZT "Hard" Pz24	400	190	0.5	0.52	/	330	(13)
$PbNb_2O_6$ Pz35	220	100	0.05	0.34	/	500	(13)
BaTiO3	1,700	190	0.36	/	0.5	115	(14) (15)
BNT	467	57-64	0.18	/	/	310	(11) (16)
BNT-$BaTiO_3$	625-776	117-125	0.28	0.43	/	288	(17) (18)
KNN	290	70-97	0.29-0.35	0.4	0.51	420	(19) (20)
KNN (HP)	420	160	0.45	/	/	/	(19)
KNN (SPS)	550	/	0.38	/	0.43	416	(21) (22)
KNN + 6% Li	500	160-235	0.42-0.45	0.49	/	450	(20) (23)
KNN + Cu	200-290	90-180	0.39	/	/	402	(24)

Alkali niobates have been generating a large amount of interest recently. These lead-free perovskite materials with the general form $ANbO_3$ (A=Alkali metal) were first investigated in the 1950s (15). One of the earliest alkaline niobates to be researched was potassium niobate ($KNbO_3$). Potassium niobate has the orthorhombic crystal structure at room temperature and relatively weak piezoelectric properties, with limited interest shown in it until recently; when in 1999 it was found that $KNbO_3$ had greatly enhanced piezoelectric properties along certain non-polar crystallographic directions than along the polar axis (25). A thickness coupling coefficient (k_t) of 0.7 was reported; considerably higher than many leading lead oxide-based piezoelectrics. These properties have been found to be stable over a large temperature range where the orthorhombic phase is stable (26). High quality $KNbO_3$ single crystals are available and are of interest for their excellent optical properties but polycrystalline $KNbO_3$ ceramics are proving difficult to fabricate by conventional methods (26). Today, $KNbO_3$ is perhaps most widely used in combination with $NaNbO_3$ in a binary system that gives one of the most promising lead-free materials.

Potassium sodium niobate, (K, Na) NbO_3 was first discovered to be ferroelectric in the 1950s. It is a solid solution of ferroelectric $KNbO_3$ and anti-ferroelectric $NaNbO_3$. The binary system $KNbO_3$-$NaNbO_3$ (Fig 1.4) is relatively complex in comparison to the PZT system (Fig 1.2), and ferroelectricity is reported up to 90% $KNbO_3$ (26). An early study (27) investigated nine different K/Na ratios and found that the composition $K_{0.5}Na_{0.5}NbO_3$ was the most promising as a piezoelectric material, in part down to a MPB that exists near the 50/50 composition separating two orthorhombic phases. Compositions in this region exhibited particularly high planar coupling and piezoelectric longitudinal response. Since then, research on KNN has been focused almost entirely on compositions with a K/Na ratio of 1. With a low density (4.51 g/cm^3) and high Curie temperature (420 °C), KNN is

appealing for a broad range of applications. Its low theoretical density contributes towards a low acoustic impedance, which is advantageous for use in transducers, particularly in underwater and medical imaging applications. In addition, it is more environmentally friendly than rival lead-free material BNT, which contains bismuth, a toxic element.

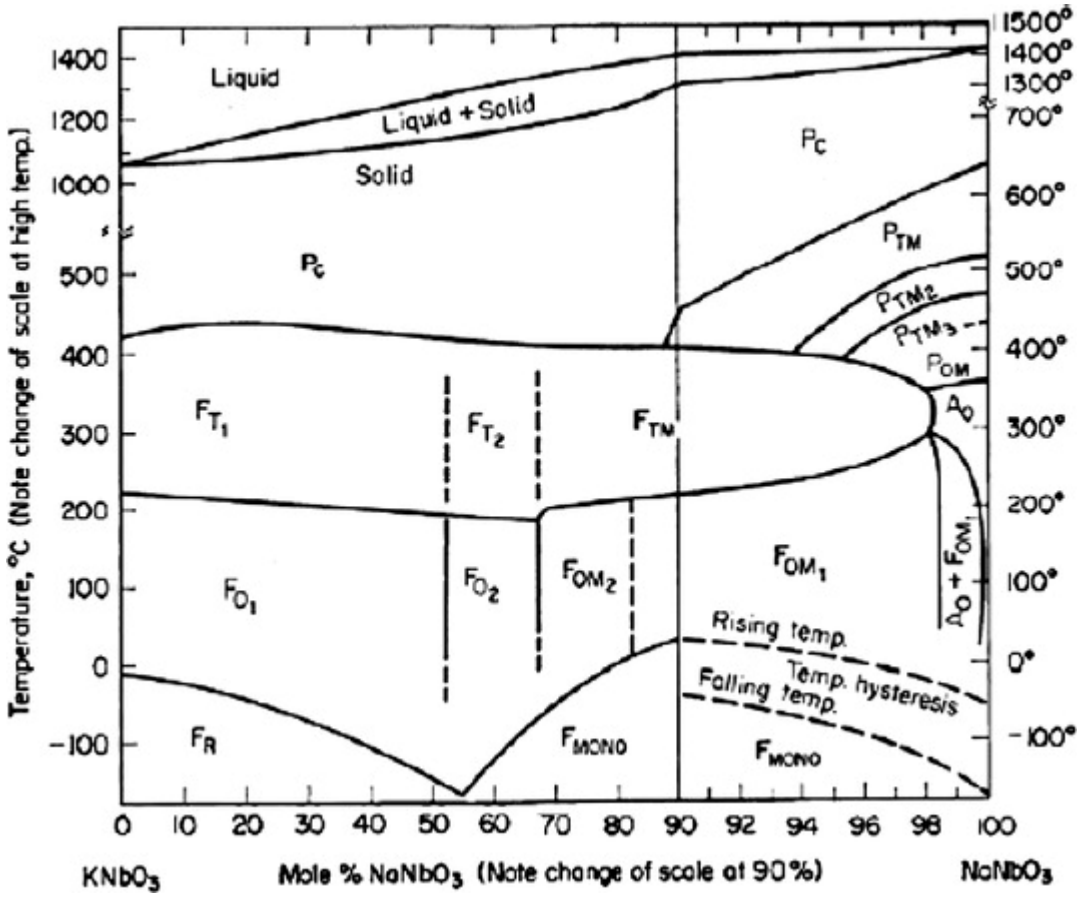

Figure 1.4 KNN phase diagram. MPB ~X=0.53, reproduced from Ringgaard et al. (31)

Comparative studies have been carried out to determine the feasibility of KNN replacing PZT and other lead-based materials in high frequency transducer applications. Feuillard et al. simulated the performance of a 10 MHz single element transducers based on KNN's material properties (28). Results were then compared to those obtained with three commercially available lead-based materials from Ferroperm Piezoceramics (13); Pz27 (a

soft-doped PZT), Pz34 (a lead titante ceramic commonly used in medical transducers) and Pz35 (a modified lead metaniobate). The KNN-transducer exhibited characteristics close to that of the Pz34 based transducer, displaying higher sensitivity than both Pz27 and Pz35. Its low dielectric constant coupled with low acoustical impedance also gives it better electrical matching than the Pz27-based transducer despite having a lower coupling coefficient than the PZT ceramic. Whilst it is important to note that PZT has a high dielectric constant and so is better suited to multi-element array transducers rather than single element transducers, the study proves that KNN could be a realistic alternative in the fabrication of operational ultrasonic transducers, and shows comparable performance to some of the lead-based ceramics currently on the market.

Up until recently, the majority of alkali niobate ceramics, KNN included had not been intensively researched since the 1970s. Whilst PZT has been studied extensively for many years and optimised both in terms of processing and dopants, a number of obstacles have prevented the further development of KNN and have limited its widespread use. The main issue encountered when fabricating KNN is the difficulty in obtaining a fully dense ceramic. The best densities achieved through conventional air sintering are between 90-95% of the theoretical density (26). A limiting factor is the phase stability of KNN, which is limited to approximately 1140 °C. Above this temperature, alkali-deficient secondary phases of tungsten bronze structure can appear and are accompanied by abnormal grain growth (29). High sintering temperatures are therefore not possible. The addition of Bi_2O_3 improves phase stability of KNN at high temperatures, but this also raises the necessary sintering temperature (30). The volatility of the alkali elements can also pose problems during sintering. Potassium or sodium loss is known to occur at elevated temperatures, which can lead to a loss of stoichiometry. KNN has piezoelectric and dielectric properties

that are sensitive to processing, and slight changes to the stoichiometry can have a marked effect on these properties. Ringgaard et al. found that the dielectric properties of KNN with 0.5 mol% excess of Nb_2O_5 vary erratically as a function of temperature at certain frequencies, compared to well-processed, stoichiometric KNN, where no frequency dispersion is apparent (31). Due to the above issues encountered when fabricating KNN, PZT and other lead-based ceramics became the dominant group of materials used in piezoelectric components.

The last decade has seen renewed interest in KNN however, and it is now the most investigated lead-free ferroelectric system of the last 5 years, surpassing bismuth alkali titanate-based materials (29). An initiative called the LEAF project ran from 2001 to 2004 with the intention of finding alternatives or replacements for conventional lead-based materials. Alkali niobates, with particular emphasis on KNN, were the main focus of this study. The main objectives of the LEAF project were to investigate ways in which the processing of KNN could be further optimised in order to obtain greater reproducibility of properties. As well as this, various dopants were trialled, in an attempt to bring KNN's piezoelectric properties on a par with those of lead-based ceramics.

Alternate methods of fabricating KNN have been looked into from an early stage. Due to the difficulty in fabricating fully dense ceramic by air sintering, a number of studies were conducted on pressure-assisted sintering. A relative density of 98.9% was achieved by hot pressing at a temperature of 1100 °C for 20 minutes (19). This improved densification resulted in coupling coefficients increasing by 20% and d_{33} values almost doubling when compared to reported values for conventionally sintered samples (see Table 1.1). Hot isostatic pressing (HIP) has also been applied to KNN, with densities of over 99% reported and a corresponding improvement in piezoelectric properties (32). More recently, spark

plasma sintering (SPS) has been increasingly used instead of hot pressing because of its advantages of a rapid heating rate and short soaking time (22). Relative densities of 98% have been obtained by SPS at temperatures ranging from 1040-1100 °C with post-annealing at 950 °C (21). The short duration of sintering and low annealing temperature results in a smaller average grain size. Whilst the density is lower than what could be obtained by hot pressing, this method yielded a higher room temperature dielectric constant and a higher coercive field, which are related to the smaller grain size that ceramics prepared by SPS possess. Within the leaf project sinter forging has also been trialled and has proven effective in obtaining very dense ceramics (31). Saito et al. have reported d_{33} values as high as 416 pC/N through fabricating texture-based KNN ceramics by a reactive grain-growth method (33), which involves introducing a preferential crystallographic orientation into the ceramic. Despite the improvement in piezoelectric properties that that these alternate fabrication techniques give, it is unlikely that any will become industrially feasible due to the high cost of the processes.

Given PZT's versatility and its ability to be used as a hard or soft material, for a single material to seriously compete with PZT over a range of different applications it would also have to be made in hard and soft variants. Both as part of the LEAF project and in independent studies, KNN has been shown to respond well to a number of different dopants, which could potentially allow its piezoelectric properties to be tailored for a specific application. Chemical modifications of KNN can generally be divided into two groups. The first group aims to improve the properties of KNN by assisting densification during the sintering stage. A number of different additives have been found to improve the sinterability of KNN-ceramics through the formation of a liquid phase. Using CuO as a sintering aid leads to the formation of a $K_4CuNb_8O_{23}$ phase with a low melting point of

1050 °C (24). The presence of a liquid phase results in a dense microstructure being developed and a relative density of 97.5% obtained. A dopant based on alkaline germanate has also been used as a sintering aid (34). This melts at a temperature of 700 °C and KNN modified with this starts to densify at temperatures almost 100 °C lower than for pure KNN, allowing for a reduction in sintering temperature to 1000 °C whilst preserving the piezoelectric properties of KNN. This helps prevent Na_2O evaporation which can occur above 1000 °C. Promoted grain growth and a relative density of 96% have been achieved through the addition of 1 mol% of ZnO to the KNN powder (35). Sintering aids can often only be used in small quantities however, as excessive amounts can lead to a degradation of the piezoelectric properties.

The second group of dopants relate to the orthorhombic to tetragonal phase transition temperature ($T_{O\text{-}T}$), which is found in pure KNN at ~200 °C (see Fig 1.4). In ferroelectric materials such as KNN, crossing a phase transition line leads to changes in the domain wall structure and thus depolarisation. To avoid this happening, it is often preferable to use modified compositions that have the $T_{O\text{-}T}$ below room temperature to reduce the likelihood of a loss of polarisation. A number of dopants are known to strengthen the tetragonal phase in KNN, thus lowering $T_{O\text{-}T}$. $CaTiO_3$, a perovskite mineral, is useful as a phase transition shifter and is effective in lowering the phase transition temperature in KNN to well below room temperature, giving a ceramic with thermally stable properties (36). Other dopants such as lithium (Li) (23), tantalum (Ta) (23) and antimony (Sb) (37) are aimed at exploiting the improved piezoelectric and dielectric properties that are associated with the O-T phase transition. These improved properties come about as a result of structural instabilities induced in the material in the region where both orthorhombic and tetragonal phases coexist (29). Guo et al. were able to fabricate Li-modified KNN ceramics that

featured greatly enhanced piezoelectric coefficients when compared to pure KNN (20), with maximum properties achieved for compositions containing ~6 mol% Li. Others have had similar success, with Hollenstein et al. reporting permittivity to almost double in KNN ceramics through lithium substitution (23). This makes lithium of particular interest as a dopant material, with one of the main drawbacks of unmodified KNN its relatively low permittivity compared to PZT and other lead-free materials, which has made it unsuitable for certain applications such as composite transducers that rely on electrical impedance matching.

These enhanced properties were initially thought to be because of an MPB. Subsequent studies however, have shown it to be because the thermally induced phase transition between orthorhombic and tetragonal phases for certain modified compositions of KNN occurs at room temperature ($T_{O\text{-}T} \approx 25$ °C) (38). As well as the enhanced piezoelectric properties associated with the O-T phase transition, Li-modified KNN is able to be fabricated to higher densities using conventional methods and has a higher Curie temperature (450 °C), making lithium one of the most promising dopant materials for KNN.

1.4 Project Aims and Objectives

The aim of this project is to determine if a lead-free ceramic can achieve comparable functional properties to PZT, and therefore be considered as a realistic alternative to the lead-based material in piezoelectric applications. The lead-free perovskite material sodium potassium niobate (KNN) is the chosen focus of this study. Its biocompatibility and low density means it could appeal to a potentially wide range of practical applications if its key properties can match those of rival lead-based materials. It has already been established however, that pure KNN fabricated by conventional methods is unable to compete with

most market leading piezoelectric ceramics, and that developing it through the use of dopants is the most promising way forward. This project will involve fabricating Li-substituted KNN ceramics from starting powders by the conventional mixed oxide method. Upon successful fabrication, structural and functional characterisation of the material will be carried out.

2. EXPERIMENTAL APPROACH

Lithium-modified (K,Na)NbO_3 ceramic samples were synthesised by the conventional mixed oxide method from raw powders, featuring an equal molar ratio of potassium(K) to sodium(Na) and A-site lithium substitution ranging from 0-9 mol% in 1 mol% increments, giving a total of ten different material compositions:

$(K_{0.5-x/2}, Na_{0.5-x/2}, Li_x)\ NbO_3$

(x=0, 0.01, 0.02, 0.03, 0.04, 0.05, 0.06, 0.07, 0.08, 0.09)

This section details the various stages in the fabrication process for both the undoped and lithium-doped samples, as well as the various physical and electrical characterisation techniques used.

2.1 Fabrication Procedure

The starting materials were as follows:

Sodium carbonate (Na_2CO_3) (≥99.5%, Sigma-Aldrich, UK)

Niobium pentoxide (Nb_2O_5) (99.9%, Sigma-Aldrich, UK)

Potassium carbonate (K_2CO_3) (≥99.0%, Sigma-Aldrich, UK)

Lithium carbonate (Li_2CO_3) (≥99.0%, Sigma-Aldrich, UK)

The powders were dried at 100 °C for 24 h in an oven prior to use to remove any contained moisture, as the carbonate precursors in particular K_2CO_3 are sensitive to moisture. The correct stoichiometric quantities of each starting powder were calculated for each of the desired material compositions, before the powders were mixed together by ball milling. They were ball milled in a plastic container with the addition of zirconia balls and ethanol

for 24 h, to ensure all powders were thoroughly mixed together. After ball milling, the zirconia balls were removed and the mixture was left in a 100 °C oven overnight (24 h) to allow the ethanol to be evaporated off.

The mixture was then ready to be calcined, a heat treatment process, to bring about phase changes including the decomposition of the carbonates to form one homogeneous powder. The mixed powder was transferred to an alumina crucible and heated at a rate of 5 °C/min to 800 °C and kept at that temperature for 5 h. The reaction that takes place is as follows:

$$0.5K_2CO_3 + 0.5Na_2CO_3 + Nb_2O_5 \Longrightarrow 2(K_{0.5}Na_{0.5})\,NbO_3 + CO_2$$

For the Li-substituted samples, there is a similar chemical reaction, where the carbonates decompose, releasing carbon dioxide as a waste product:

$$(0.5\text{-}x/2)K_2CO_3 + (0.5\text{-}x/2)Na_2CO_3 + xLiCO_3 + Nb_2O_5 \Longrightarrow 2K_{0.5-x/2}Na_{0.5-x/2}Li_x + NbO_3 + CO_2$$

X-ray Diffraction was used to identify the crystalline phases present after calcination. Slight changes to the stoichiometry of the KNN powder can result in the formation of hygroscopic secondary phases that can lead to disintegration of the ceramic during sintering. Therefore, XRD is an important step in confirming the powder has completely reacted to form one homogeneous powder that can then be further processed. Crystallographic analysis was carried out using a Philips X'Pert diffractometer that uses a CuKα X-ray source.

The calcined powder was then remilled. A vibratory mill was used to break up any agglomerate particles and thus reduce the overall particle size of the powder. A container of the coarse calcined powder was placed in the vibratory mill for 48 h. In addition to the KNN powder, ethanol and zirconia balls were added to act as the grinding interface. Hard

and unlikely to contaminate the powder, they would hopefully break the powder down to a finer particle size.

After the powder was removed from the vibratory mill it was placed in an 80 °C oven to dry out before undergoing a stage of sieving. The sieving process ensures the KNN powder is of acceptable particle size to continue with the fabrication. The sieve consisted of three trays going from 106 μm spacing to 63 μm and finally 38 μm. Zirconia balls were again added for each layer before the sieve was placed in a sieve shaker that acts in a similar manner to the vibratory mill, by vibrating, causing all the KNN powder to fall to the final container. This should guarantee a maximum particle size of 38 μm but to get a clearer indication of the particle size distribution, a particle size analyser (HELOS Laser Diffraction Series, Sympatec GmbH) was used. This works by laser diffraction, where a laser light interacts with the dispersed powder particles, and the differing diffraction patterns represent the different sized particles. This provides quantitative data, giving a trace of volume size distribution and cumulative distribution. On the first fabrication run through (for pure KNN), the particle size analyser was used after the powder was calcined, and once again after the powder had been milled and sieved, to ensure the efforts to reduce the particle size had been successful. Once this had been confirmed, particle size analysis was done only after the milling and sieving stages for the subsequent compositions.

Before being pressed, binder was added to the calcined powder to aid with compaction. Different binders were trialled, including polyvinyl alcohol (PVA). The calcined powders were mixed with 2 wt% PVA prior to being compacted. Unfortunately the samples that had a PVA addition featured large surface voids post-sintering, where the binder had burnt out but the sample had not densified sufficiently enough to eradicate these voids. This may have been down to the relatively coarse grain size of the PVA when compared to the

calcined powder. Fabricating samples with no binder addition was also investigated. Whilst they appeared to sinter well, the extremely low green strength of samples without binder made handling and analysing the samples in their pre-sintered state difficult. A combination of Duramax B-1000 and B-1007 (aqueous emulsion, Chesham Chemicals Ltd., UK) water-based binders gave a ceramic with high green strength and no issues arose during sintering, with the binder burning out cleanly.

The calcined powder, with the addition of 3 wt% B-1000 and 2 wt% B-1007, was mixed for 24 h then dried, before the processed powder was compacted into shape by a powder press. This involved inserting the powder into a 13 mm diameter die, before a pressure of 100 MPa was applied for 30 seconds. Disc-shaped powder compacts were ejected from the die cavity, approximately 0.5 g in weight and 1 mm in thickness.

In order to achieve full densification of the green powder compacts, sintering is required. The sintering process involves consolidating the powder particles by heating the powder compacts to a high temperature below the melting point. This provides the necessary energy to encourage the individual powder particles to bond together, removing any porosity present from the compaction stage. The sintering was carried out in a box furnace (Lenton Furnaces, UK) in air. This step can be problematic as phase stability is limited to ~1140 °C for KNN and sodium evaporation at high temperatures is also a known issue (26). The dwell time was also carefully considered as too long a dwell time could lead to excessive grain growth and Na loss, whilst too short a time would result in insufficient densification. With this in mind, the samples were sintered with a dwell time of two hours in a covered alumina crucible to limit the sodium loss as much as possible. A sintering temperature of 1050 °C was initially trialled but found to provide inadequate densification to the samples so this was increased to 1100 °C. This is considered the upper limit when

sintering KNN ceramics, as any higher would risk phase instabilities and a loss of stoichiometry.

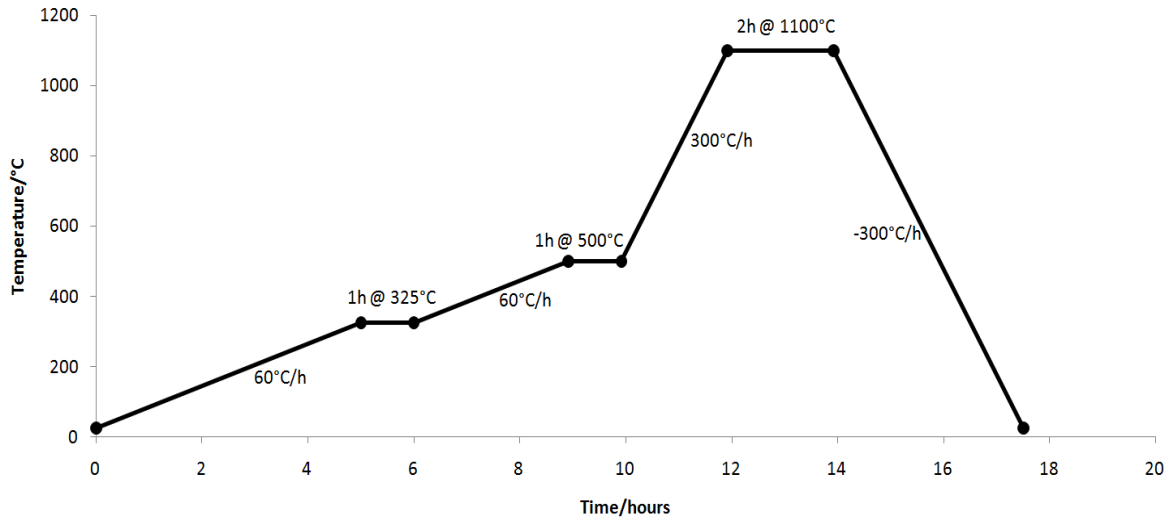

Figure 2.1 Schematic diagram of the sintering program for the green samples

The sintering was carried out in stages (Fig 2.1). Initially the samples were heated up to 325 °C at a ramp rate of 60 °C/h and held at this temperature for one hour to burn out the binder. The temperature was then increased to 500 °C at the same ramp rate and held for a further one hour. Finally, the temperature was raised to the target sintering temperature of 1100 °C at an increased ramp rate of 300 °C/h. After a dwell period of two hours, the samples were cooled to room temperature at a rate of 300 °C/h. It is important to control the heating rate carefully as it influences the grain growth rate and therefore effects the microstructure and density of the sintered ceramic.

The density of the sintered discs was determined using a water immersion technique based on the Archimedes' principle, which states that the buoyant force on a submerged object is equal to the weight of the liquid displaced by the object. By taking two measurements; the mass of the sample when dry and the mass of the sample when submerged in water, the

volume of the sample can be determined (Equation 2.1). From that, the density of each sample could be calculated (Equation 2.2).

$$V = \frac{\mathrm{m} - \mathrm{m}'}{\rho_{water}} \qquad \text{Equation 2.1}$$

where V is sample volume, m is sample mass, m′ is sample mass when submerged, and ρ_{water} *is the density of water, taken as 1 g/cm*^{3}.

$$\rho_{\mathrm{sample}} = \frac{\mathrm{m}}{V} \qquad \text{Equation 2.2}$$

where ρ_{sample} *is the sample density, m is sample mass and V is sample volume.*

The chemical and structural properties of the ceramic samples were examined by X-ray diffraction (Philips X'Pert, Netherlands) and scanning electron microscopy (JSM 6060, JEOL, Japan). Sample preparation for SEM fracture surface analysis involved attaching the samples to stainless steel stubs using carbon adhesive tape. A 75 nm thick gold layer was then sputter coated onto the samples to create the required electrical contact. SEM analysis of the starting powders and milled calcined powder was also carried out.

In preparation for functional characterisation, the samples were ground and polished to a thickness of 0.5 mm, giving the samples a suitable aspect ratio (thickness/diameter) of 0.05 for the subsequent functional measurements. Samples were then electroded by sputtering gold onto both parallel faces of the discs. Thin strips of PVC tape were cut with a scalpel blade then wound around the edge of the samples prior to electroding. This ensured the gold did not cover the sample edges, thus keeping the face electrodes isolated from each other to prevent electrical shorting.

The final step in preparing the samples for functional characterisation was a poling treatment. Before the ceramic can function as a piezoelectric material, it must first be

poled. This process involves aligning the domains within the material so they point in the same direction. This is accomplished by subjecting the material to a high electric field at elevated temperatures. The domains in the material are forced to align parallel to the field lines produced. After the removal of the electric field, the domains lose some alignment, but enough orientation remains to allow the material to exhibit piezoelectric properties.

The electroded samples underwent poling whilst immersed in an oil bath at 110 °C. The samples were sandwiched between a metal pin and plate and a voltage was applied directly to the ceramic for 10 minutes to ensure full domain alignment. 3 kV/mm was found to be adequate voltage to fully pole the samples. Higher poling voltages were not found to offer any advantage upon electrical characterisation and also risked destroying the sample during poling. A second technique known as Corona poling was also used to pole some of the samples. This differs from the oil poling as the process takes place in an environment of air and the electric field is not directly applied to the sample, instead a needle is suspended above the sample, which is situated on a ground plate. The applied voltage then travels through the needle and ionises the air within the chamber and a charge builds up on the sample. As the needle is not in direct contact with the sample, higher voltages can be applied without a risk to the sample, in theory allowing for a greater degree of poling. The poling process was carried out at 100 ºC with an applied voltage of 30 kV, as molecular mobility increases with temperature, enabling the rotation of domains to occur more readily.

2.2 Electrical Characterisation

Characterisation of the poled samples was carried out 48 h after poling to minimise aging effects. The functional properties of the ceramic were determined using various measurement tools.

A precision impedance analyser (Agilent 4294A) was used to measure the electrical impedance and capacitance of the material as a function of frequency. The samples were loaded into a measurement jig attached to the analyser and placed in contact with a pin. At certain frequencies, a piezoelectric material enters a resonant mode where the electrical input signal excites a mechanical response within the material. These resonant modes are what make a piezoelectric material unique, and are not present in dielectric materials. Each time the material enters this state, a resonance and anti-resonance will exist where the impedance behaves in a well defined manner. A pair of critical frequencies can be identified. The resonance frequency, defined as the frequency of maximum admittance is the lower of the critical frequencies (f_r). The antiresonance, defined as the frequency of maximum impedance, is the upper critical frequency (f_a).

Figure 2.2 shows a typical impedance plot for a piezoelectric material. When measuring electrical impedance, the analyser outputs a data trace showing impedance (Ω) and phase (º) over a specified frequency range. Note the region of the graph where the sample enters resonant mode ~330 kHz.

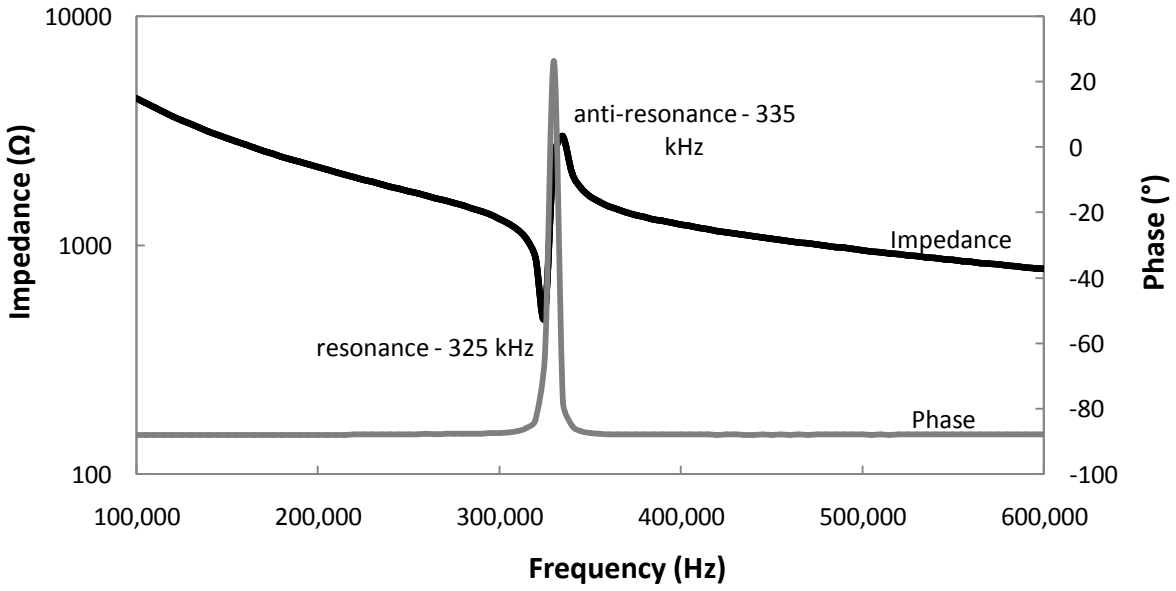

Figure 2.2 An impedance(Z) and phase(°) trace extracted from the impedance analyser

The electromechanical coupling coefficients k_p and k_t are two important piezoelectric parameters that quantify how efficient the piezoelectric material is in converting mechanical energy into electrical energy by relating the electrical energy output to the total mechanical energy input or vice versa. These coupling coefficients are the ones best suited for thin disc samples like the ones that have been fabricated. Other coupling coefficients exist for ceramic samples of different aspect ratios.

The planar coupling coefficient (k_p), expresses radial coupling - the coupling between an electric field parallel to the direction in which the ceramic is polarised, and mechanical vibrations perpendicular to the direction in which the ceramic is polarised.

The thickness coupling coefficient (k_t) expresses the coupling between an electric field parallel to the direction in which the ceramic is polarised, and mechanical vibrations in the same direction.

In accordance with the IEEE standards on piezoelectricity, the coupling coefficients were calculated from the resonance and anti-resonance frequencies using Equation 2.3.

$$k^2 \approx \frac{f_a^2 - f_r^2}{f_a^2}$$ Equation 2.3

The samples were analysed over a frequency range of 0-5 MHz, where resonances relating to both coupling coefficients occur. The coefficient (k_p) can be calculated by analysing the resonant mode that occurs at around 300 kHz in the samples due to lateral vibrations. The thickness mode resonance, relevant to the coefficient (k_t), occurs at 3 MHz.

The permittivity is another important property of a piezoelectric material and is a measure of how much electrical potential energy can be stored in a given volume of the material under the influence of an electric field. The permittivity is often reported relative to the permittivity of free space (ε_0) as relative permittivity (ε_r), also known as the dielectric constant.

Three separate relative permittivity values were calculated for each material composition using capacitance readings from three different frequencies. This should give an idea of how the material performs over a range of operating frequencies. Once capacitance measurements for 100 kHz, 1 MHz and 15 MHz had been retrieved from the impedance analyser the values were input into Equation 2.4 to obtain a value for $\mathcal{E}_r$.

$$\varepsilon_r = \frac{Cd}{A\varepsilon_0} \qquad \text{Equation 2.4}$$

where C is the measured capacitance, d is the sample thickness, A is the surface area, and $\mathcal{E}_0$ is the permittivity of free space, taken as 8.854×10^{-12}.

Figure 2.3 shows a typical capacitance plot for a piezoelectric material. Note the region of the graph where the sample enters resonant mode ~220 kHz. When taking a capacitance reading for calculating ε_r, this region is avoided due to the instability of the capacitance. The ideal place to take a reading is in a frequency region where the capacitance is relatively stable.

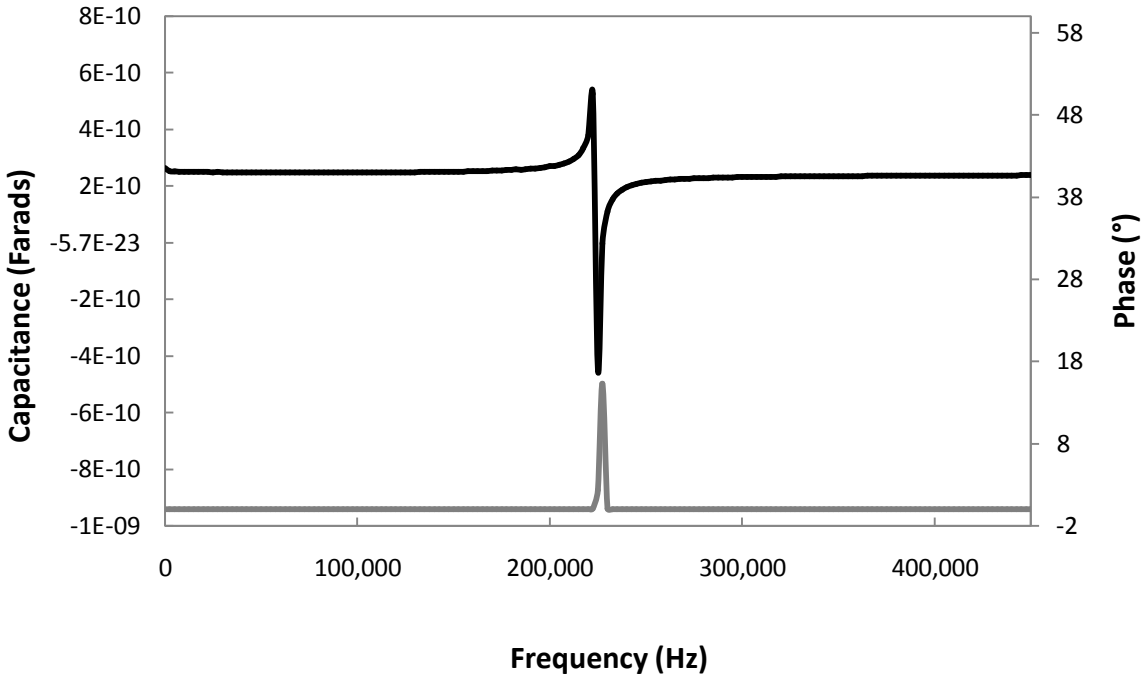

Figure 2.3 A typical capacitance trace

The final parameter to be determined was the piezoelectric charge constant d_{33}, which quantifies the longitudinal charge generated per unit of mechanical stress applied to the material. The first subscript to d denotes the direction of the charge generated in the material. The second subscript denotes the direction of the applied stress. In both instances this direction (direction 3) is parallel to the direction in which the piezoelectric material was poled.

An instrument called a d_{33} meter (Fig 2.4) was used to directly measure the d_{33}. The sample was clamped between two pins so that each face was in contact with a pin. A stress was then applied to the sample and the resultant longitudinal charge density was measured and a reading taken off the machine.

Figure 2.4 A d_{33} meter with attached apparatus for holding specimen

3. RESULTS AND DISCUSSION

Results were gathered throughout the fabrication process. Structural and chemical analysis was undertaken when the material was in powder form, and then further analysis took place on the material once sintered. Finally, once electroded and poled, the materials key functional properties were determined.

3.1 Precursor analysis

3.1.1 XRD traces of starting powders:

Figures 3.1-3.3 below show X-Ray diffraction plots of the three KNN precursor materials.

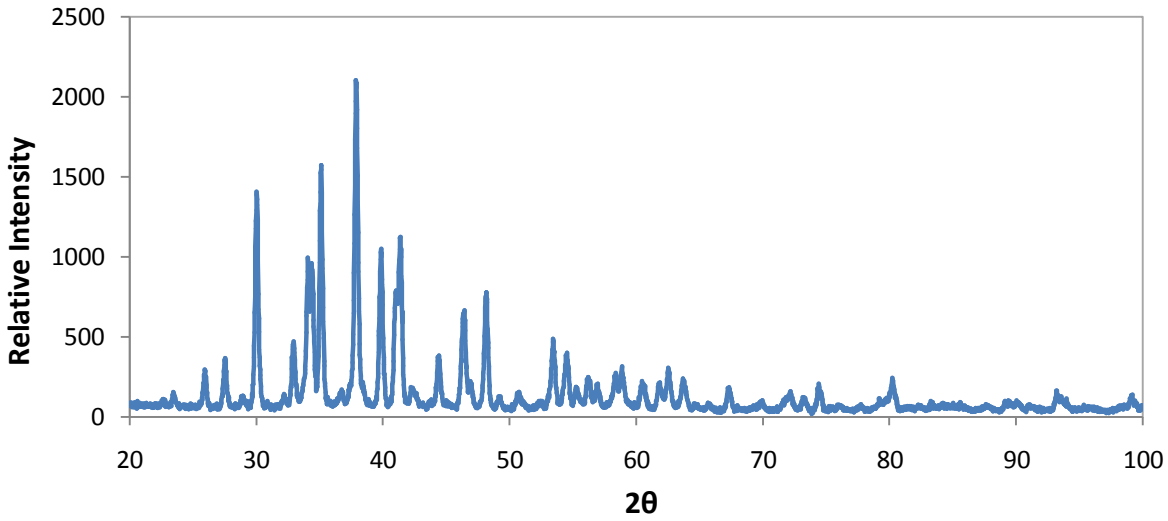

Figure 3.1 X-ray diffraction pattern of Na_2CO_3 powder

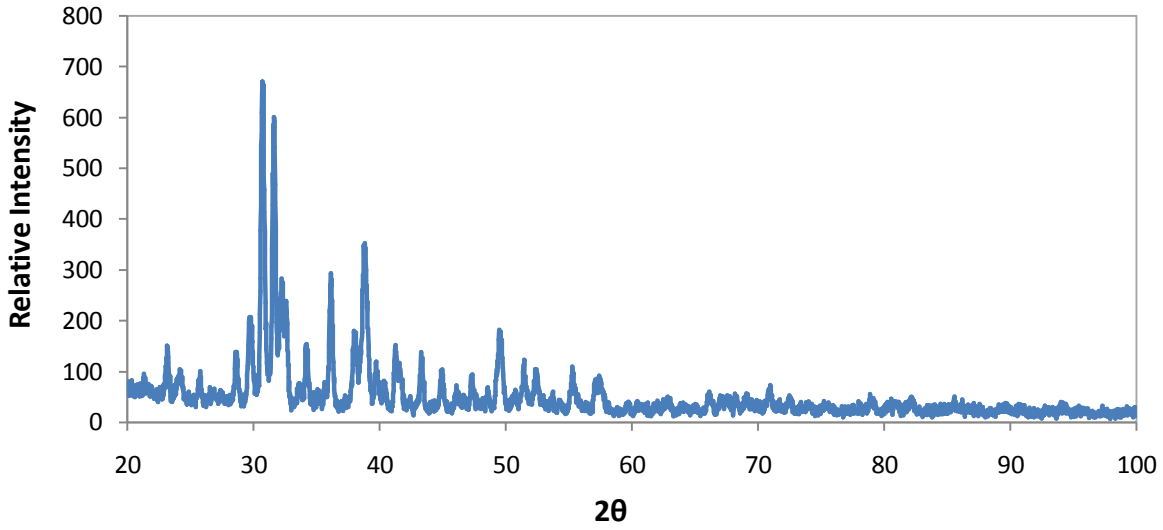

Figure 3.2 X-ray diffraction pattern of K_2CO_3 powder

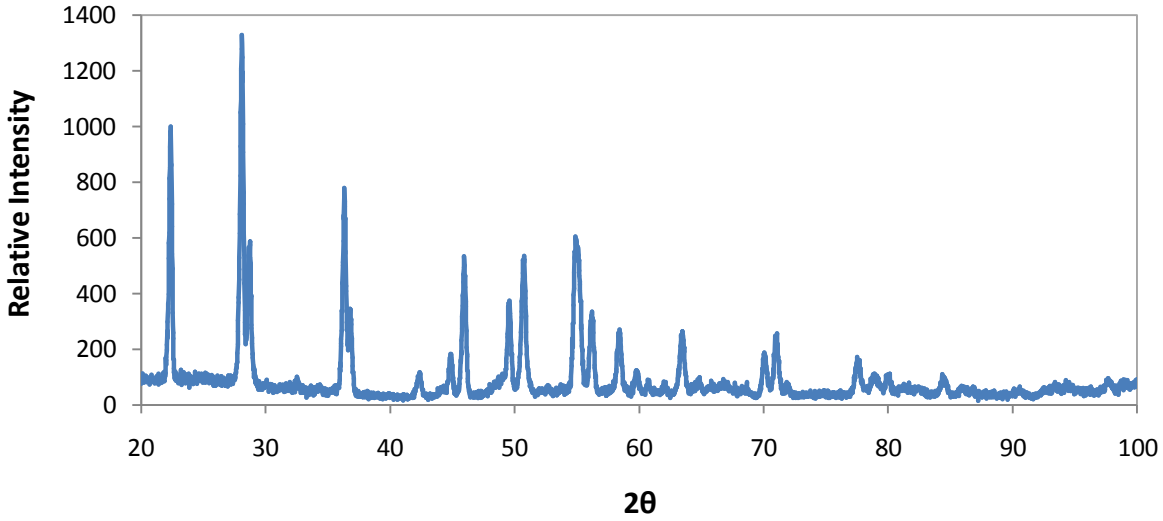

Figure 3.3 X-ray diffraction pattern of Nb_2O_5

3.1.2 Micrographs of starting powders

Figures 3.4-3.6 show SEM micrographs of the KNN precursor materials prior to mixing.

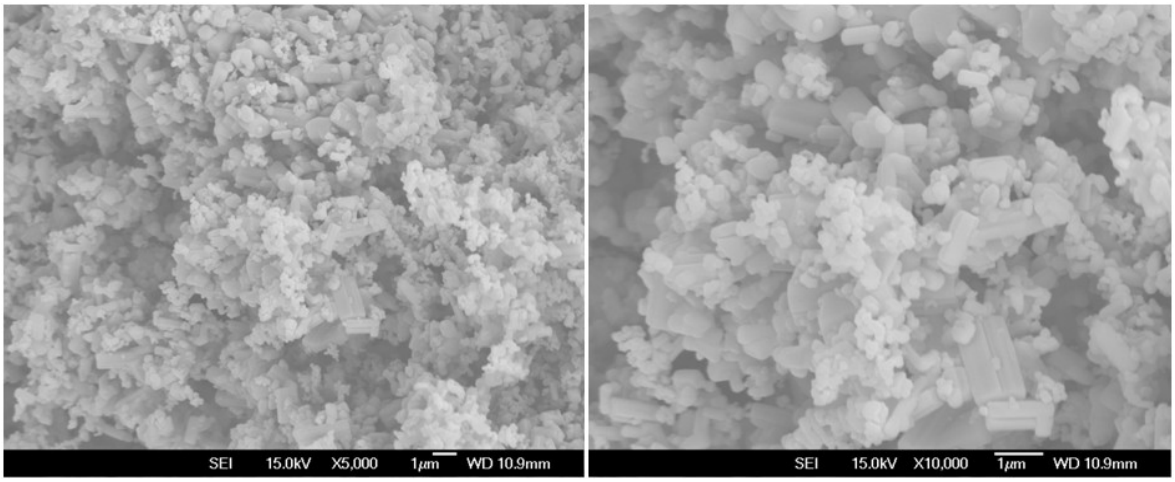

Figure 3.4 SEM images of Nb_2O_5 powder

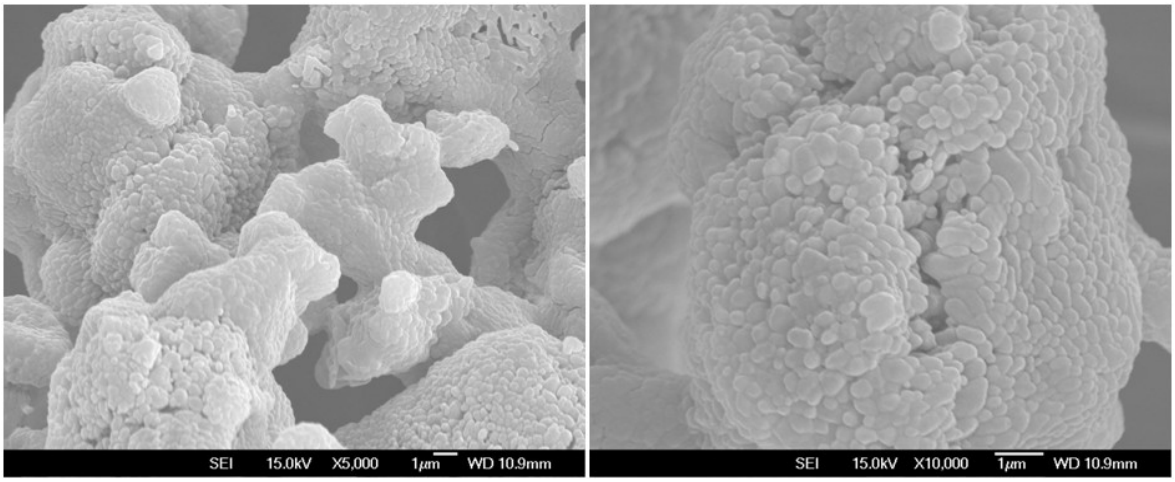

Figure 3.5 SEM images of K_2CO_3 powder

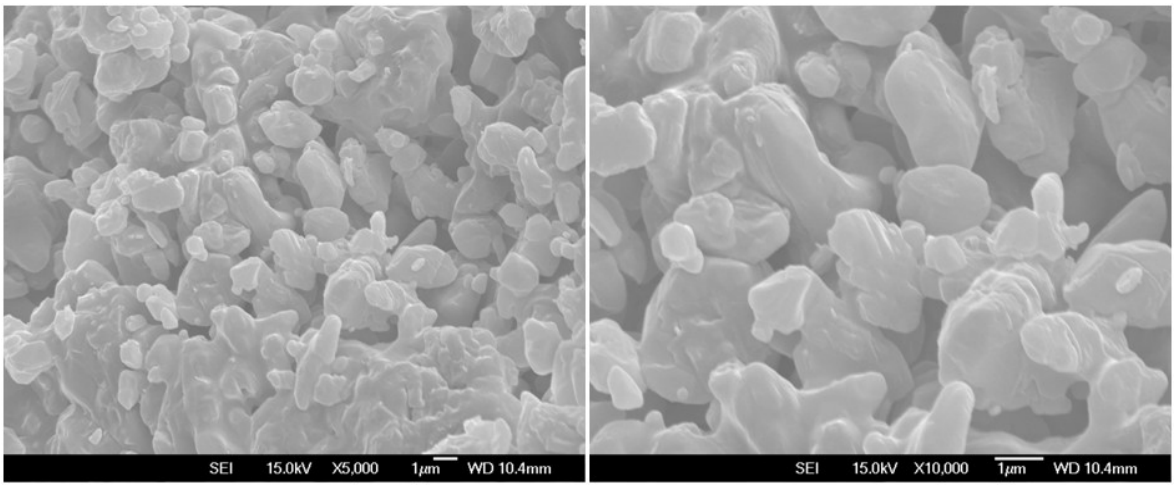

Figure 3.6 SEM images of Na_2CO_3 powder

These SEM images show a considerable contrast between each of the powders. Niobium pentoxide (Fig 3.4) is a fine powder, with a high percentage of particles under 1 µm in diameter. There is also the presence of larger cylindrical shaped grains interspersed in the powder. Potassium carbonate (Fig 3.5) is a heavily agglomerated powder of small particle size (<1 µm), and agglomerates of over 10 µm in diameter. Finally, sodium carbonate (Fig 3.6) is a coarse powder with particles ranging from 1 µm to over 10 µm in diameter, with very little uniformity in size or shape apparent.

3.2 Calcined powder analysis

3.2.1 XRD trace of calcined powder

Figure 3.7 shows the X-Ray Diffraction pattern for KNN powder after it had been calcined.

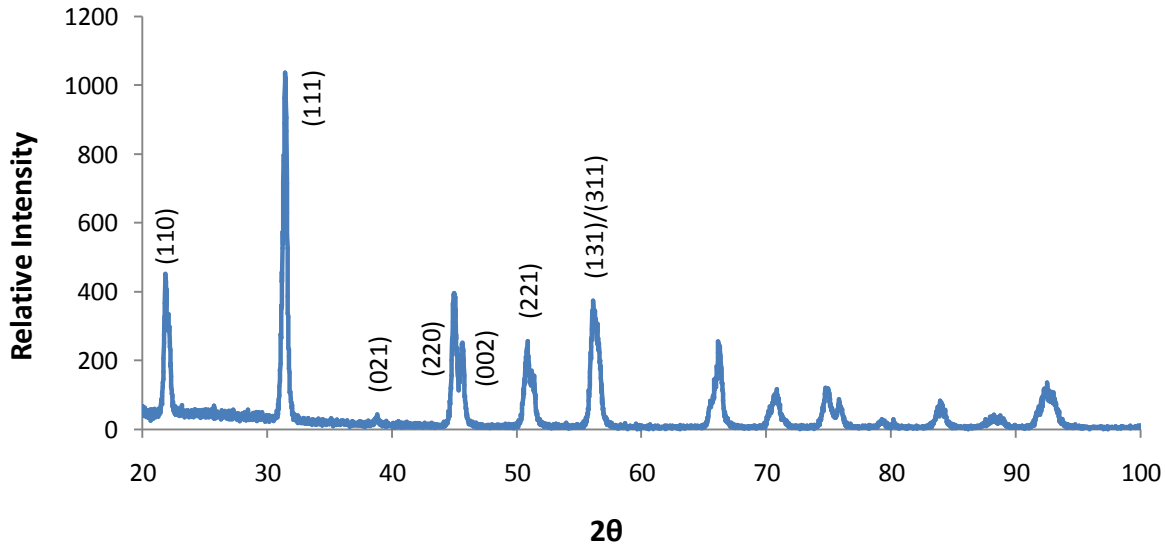

Figure 3.7 X-ray diffraction plot of KNN powder

The diffraction pattern shows peaks corresponding to a single perovskite phase. The peaks represent a fully orthorhombic structure, which is the crystal structure KNN is known to exhibit at room temperature, with no secondary phases detected. KNN powder is sensitive to stoichiometry and only slight deviations can lead to non-perovskite secondary phases.

This provides a good indication that the calcination process was successful and the powder is one homogeneous material.

3.2.2 Micrographs of calcined powder

Microstructural analysis (SEM) of KNN powder was carried out. Figure 3.8 shows SEM micrographs of calcined $(K_{0.5}, Na_{0.5})NbO_3$ powder.

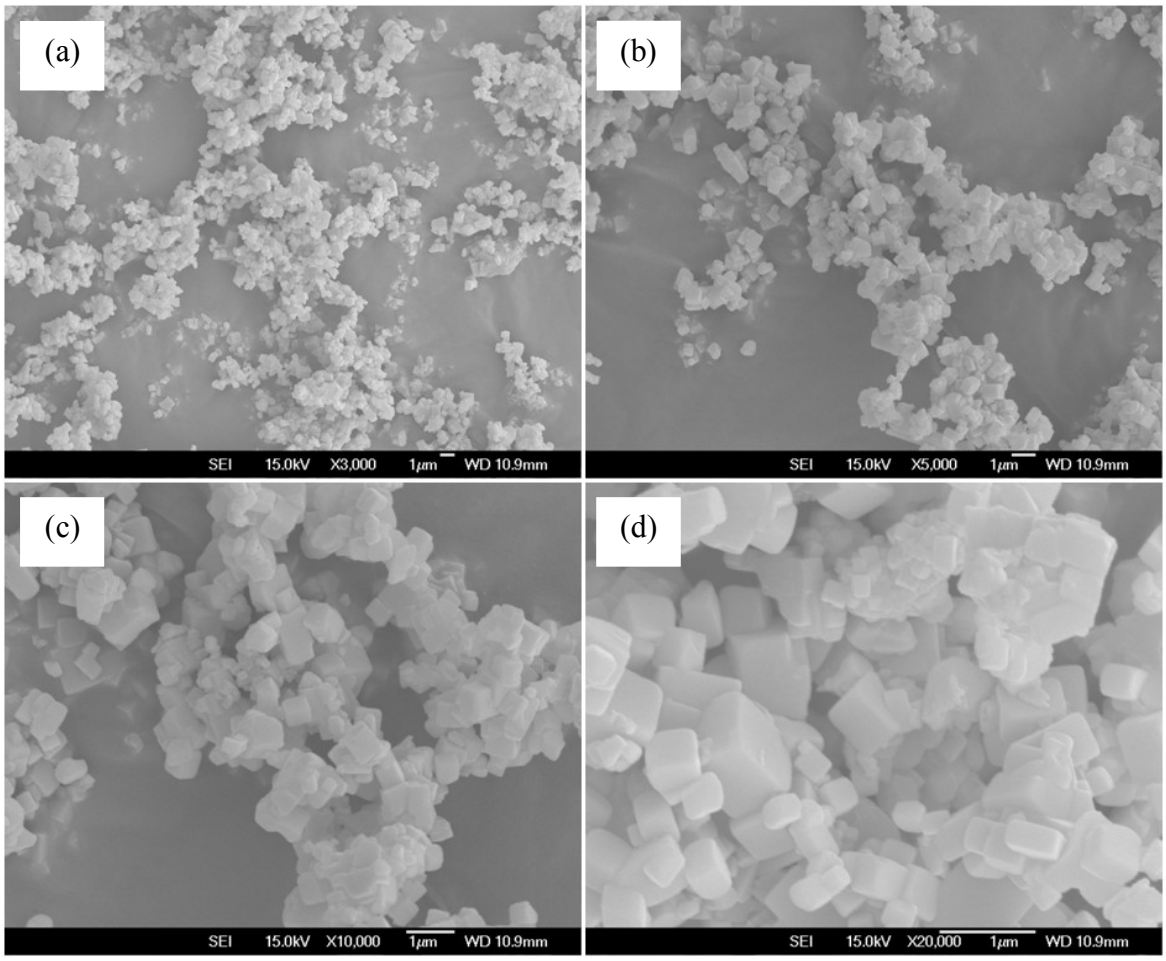

Figure 3.8 SEM images of $(K_{0.5}, Na_{0.5})NbO_3$ powder calcined at 800 °C for 5 h

SEM analysis of the vibratory-milled powder shows the KNN powder particles as having a cubic morphology, with a large proportion of them under 1 μm (Fig 3.8). Particle size analysis confirms this (Fig 3.9), with a mean particle size of 1.9 μm and no particles present over the size of 10 μm after vibratory milling. When compared to the initial powders, the calcined powder most closely resembles the niobium pentoxide powder (Fig

3.4), sharing a similar particle size and shape. This is to be expected as niobium pentoxide makes up the bulk of the calcined KNN powder in wt% terms.

3.2.3 Particle size of calcined powder before and after milling

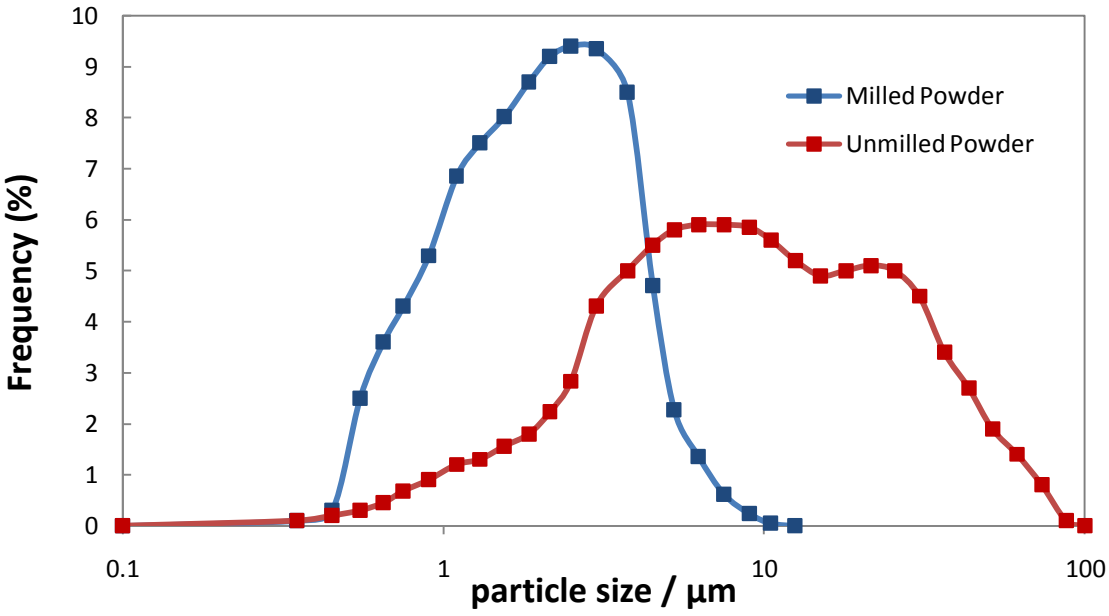

Figure 3.9 Size frequency distribution of unmilled and milled KNN powder particles

As discussed previously, vibratory milling was carried out directly after the powder was calcined. Figure 3.9 shows the effects of this milling. Directly after calcination the unmilled powder had particles ranging in diameter from under 1 µm to close to 100 µm. The results from particle size analysis confirm that vibratory milling for 48 h and then sieving had the desired effect of reducing the overall particle size, with no particles over 10 µm in diameter present in the milled powder. This small particle size is beneficial when it comes to sintering the powder, reducing the risk of any defects within the finished ceramic body.

3.3 Sintered ceramic analysis

Once the KNN ceramics had been sintered at 1100 °C, chemical analysis was carried out by X-ray diffraction, the density was calculated using the Archimedes method and microstructural analysis (SEM) was carried out as described in Chapter 2.

3.3.1 X-ray diffraction analysis of Li-modified KNN ceramics.

The crystal structure of the sintered samples was examined using XRD analysis and the diffraction patterns are shown in Figure 3.10.

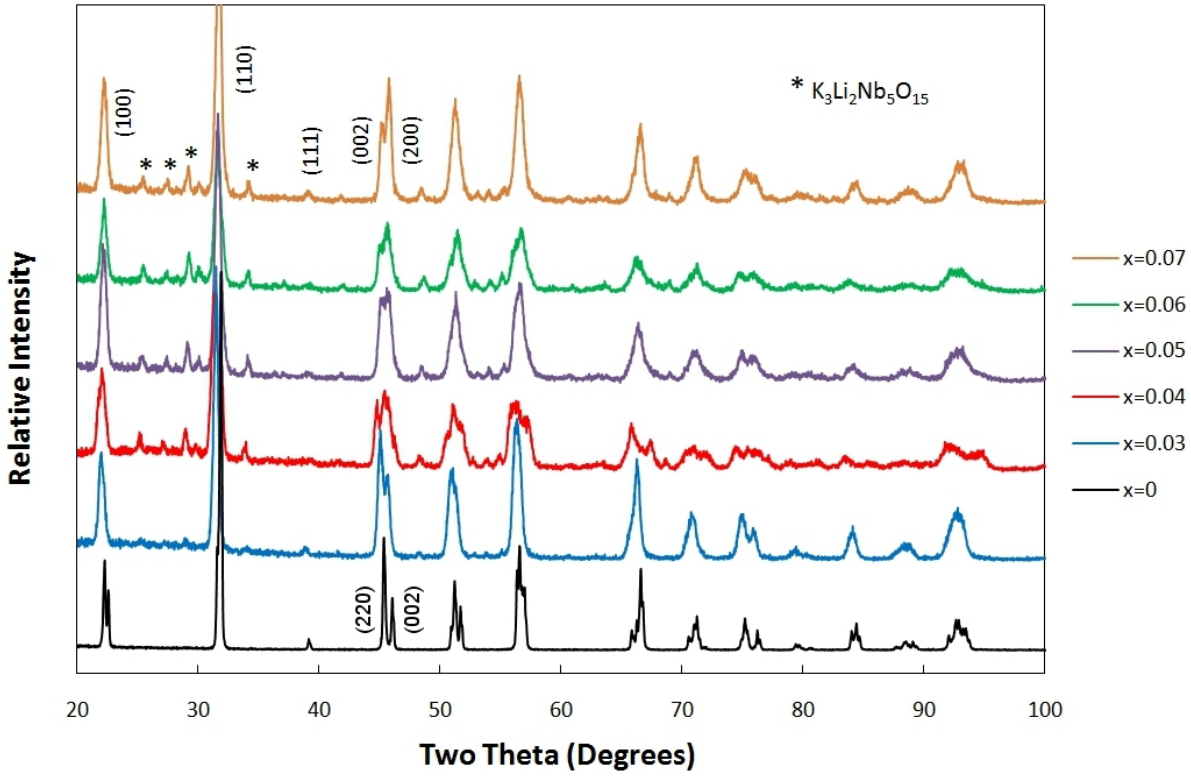

Figure 3.10 X-ray diffraction patterns of (K0.5-x/2, Na0.5-x/2, Lix)NbO3 compositions

At low lithium concentrations (x<0.04), diffraction peaks corresponding to a pure perovskite-type phase are detected, which has orthorhombic symmetry at room temperature. No secondary phases were identified, indicating that the lithium addition has

completely diffused into the KNN lattice to form a homogeneous composition. Note though that the limit of detection for XRD is ~5%. As reported in literatures (39), the orthorhombic phase is characterised by the (220)/(002) peak splitting at ~45° which is visible in both the x=0 and x=0.03 diffraction plots. At x=0.04 however, the split peak at ~45° has a reversal of magnitude, which is symptomatic of a phase transformation from orthorhombic to tetragonal crystal structure. In unmodified KNN, the tetragonal crystal structure only exists between 200 and 420 °C, but the lithium addition stabilises the tetragonal phase, decreasing the orthorhombic to tetragonal phase transition temperature ($T_{O\text{-}T}$) and enabling the tetragonal crystal structure to exist at room temperature with a high enough lithium content. Further to this, three additional peaks are registered between 20-30° for $0.04 \leq x \leq 0.07$. These particular peaks could not be attributed to any particular phase, but have previously been identified as $K_3Li_2Nb_5O_{15}$, a tetragonal tungsten bronze structure with a theoretical density of 4.376 g/cm^3, by Guo et al. (20). The existence of this secondary phase is thought to be due to the lithium content reaching its solubility limit in the A sites of the KNN ceramics. At x=0.07, most of the peaks present on the trace are sharper in appearance, and the split peak at ~45° is more pronounced, indicating the tetragonal crystal structure is now the dominant one.

3.3.2 Density

The density of the sintered samples was found to increase gradually with the introduction of lithium, with a peak density obtained at 7 mol% Li content. Table 3.1 displays the mean densities obtained for each of the ten compositions. Due to the substitution of K and Na for Li in the doped samples, the theoretical density will differ slightly for each composition. Theoretical density was therefore calculated for each individual composition, so the relative densities displayed in Table 3.1 provide a true reflection of the effect lithium has on the densification of the ceramic.

Table 3.1 Obtained densities for KNN ceramics

Li (mol%)	0	1	2	3	4	5	6	7	8	9
Density (g/cm^3)	3.85	3.85	3.88	3.91	3.93	3.99	4.08	4.14	4.07	4.08
Relative Density (%)	85.4	85.3	86.0	86.5	86.9	88.3	90.2	91.6	90.0	90.1

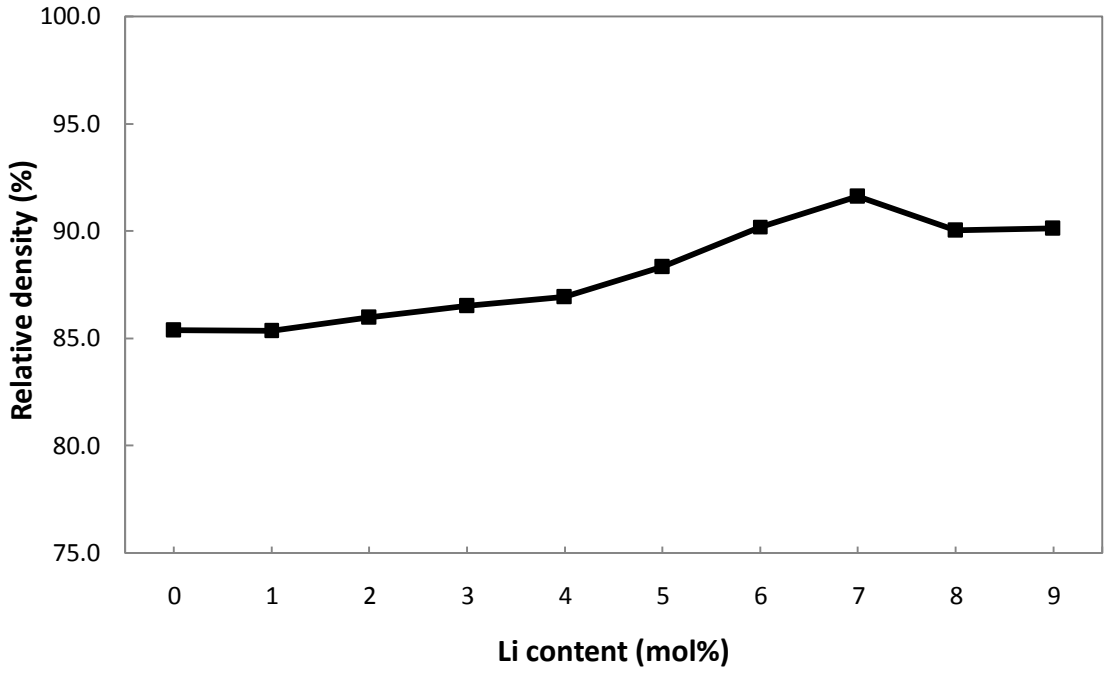

Figure 3.11 Relative densities of Li-substituted KNN ceramics as a function of lithium content

Despite a slight initial reduction in relative density with the presence of 1 mol% lithium, further lithium substitution results in a steady increase of relative density, peaking at 7 mol% Li before a decrease in density is observed for the final two compositions (Fig 3.11). The reduced density at 8-9 mol% lithium content may be attributed to the possible existence of a secondary phase $K_3Li_2Nb_5O_{15}$ (4.376 g/cm^3). This secondary phase is of a lower density than KNN and peaks thought to correspond to this phase were identified through XRD analysis (Fig 3.10). Whilst these peaks were first detected at 4 mol% Li content by XRD, it is not until the lithium content reaches 8 mol% that there is a drop in density. As well as the existence of a secondary phase, at Li concentrations >7 mol% the

ceramic is likely to be fully transformed into the tetragonal crystal structure which could also be impacting density.

3.3.3 Sintered microstructures

SEM micrographs of fracture surfaces of KNN samples with lithium contents of 0, 3, 5 and 7 mol% are shown in Figure 3.12.

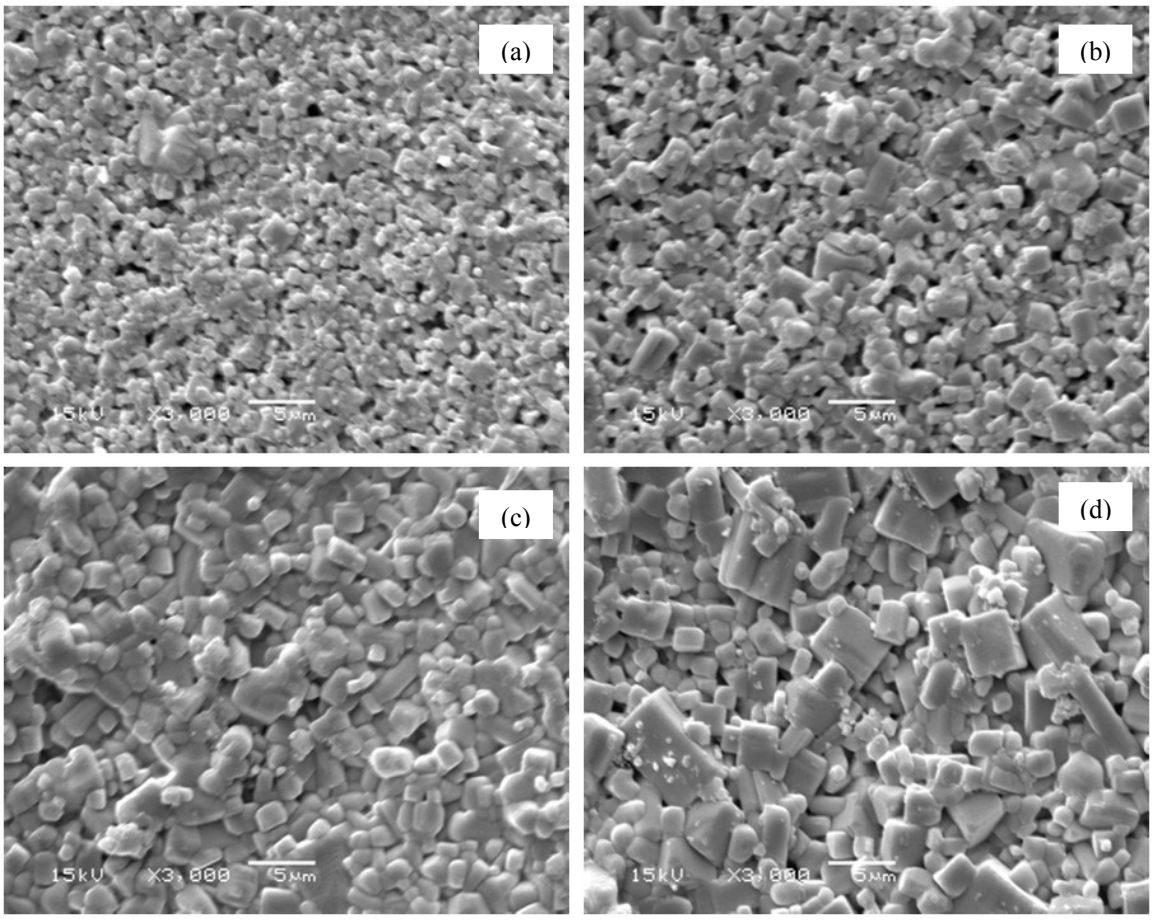

Figure 3.12 SEM fracture surface images of Li-substituted KNN ceramics sintered at 1100 °C
(a) 0 mol% (b) 3 mol% (c) 5 mol% (d) 7 mol%

The undoped KNN sample (0 mol%) has a fine-grained microstructure (Fig 3.12). When compared to SEM micrographs of the KNN in powder form (Fig 3.8), the grain growth during sintering appears to have been limited, with many grains below 1 μm in size still present. With a 3 mol% Li content, there are signs the lithium is having an effect on the microstructure. A similar microstructure is observed, but with the smaller grains

interspersed with larger grains of 3-4 μm in size. Grain size continues to increase with lithium concentration, and the sample with a 5 mol% Li content has noticeably less submicron grains present. With the lithium concentration at 7 mol%, a number of large, cubic grains ≥5 μm in size are now visible.

These results appear to show that lithium promotes an enlarged grain size upon sintering, with others also reporting similar findings (40). The results also show a relationship between sample density and grain size, with the higher density of the Li-doped samples possibly being an influencing factor on the changes to the microstructure.

3.4 Functional Characterisation

After sputtering the electrodes onto both faces of the sample, and poling, the piezoelectric properties for Li-modified KNN (0-9 mol%) were determined.

3.4.1 Piezoelectric coefficient (d_{33})

The results obtained for d_{33} for each composition are shown in Figure 3.13.

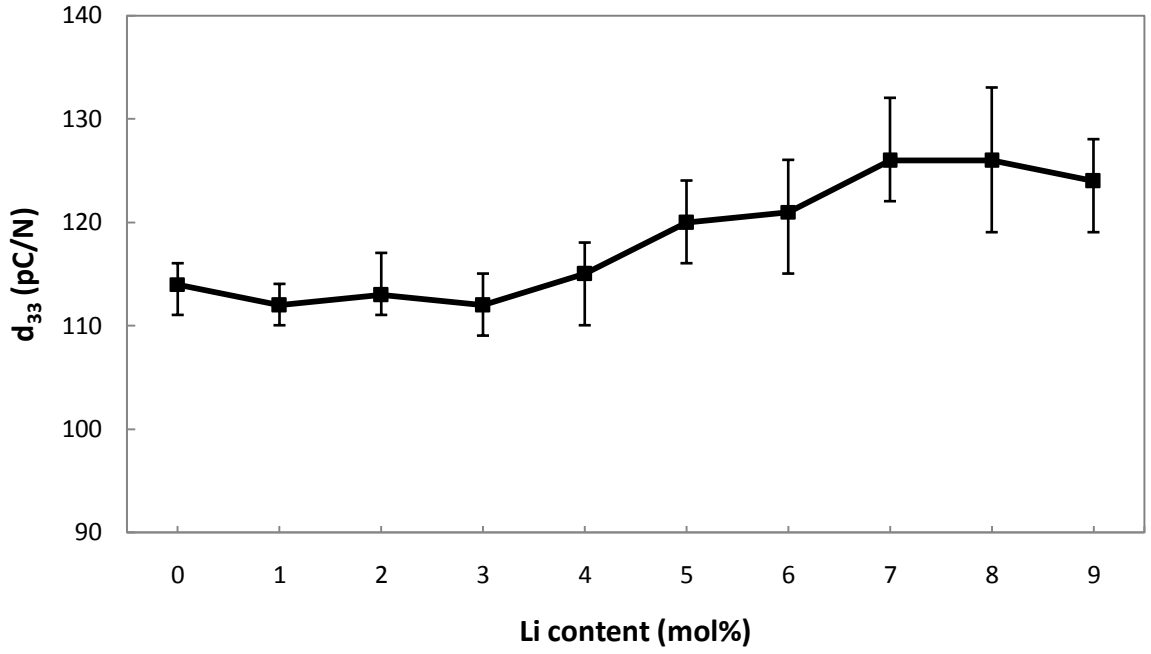

Figure 3.13 Piezoelectric coefficient d_{33} of Li-substituted KNN as a function of lithium content

A number of readings were taken for each composition, with the mean reading plotted on the graph. The error bars reflect the highest and lowest readings that were acquired over the course of testing multiple samples for each composition. This highlights the inconsistencies of taking a d_{33} reading, as the machine is very sensitive to sample geometry, specifically thickness, and the pressure applied on the sample. As the pins were manually tightened to fix the sample in place, it can be assumed that human error came into play and not all samples were examined under identical conditions. In order to reduce the influence of these variables, a large number of readings were taken and multiple samples were tested of each composition.

Despite the issues encountered whilst carrying out the measurements, a number of things can be deduced from the obtained readings. For compositions in the range 1-4 mol% Li, the presence of lithium has no apparent effect on the piezoelectric coefficient d_{33}, despite the improved densities compared to undoped samples. Hollenstein et al. have reported results consistent with those in Figure 3.13, where d_{33} was found to be independent of Li-substitution below 6 mol%, and steeply increased at 6.5 mol% (23). For compositions with >4 mol% Li, d_{33} values steadily increased with lithium content, peaking at 7-8 mol% of Li. A maximum d_{33} value of 126 pC/N was obtained, compared to 114 pC/N for the undoped samples, although the associated error bars for the optimum d_{33} compositions were comparatively large. When compared to most literature values, the results obtained are low. Guo et al. obtained a max d_{33} value of 235 pC/N (20) and Liu et al. 210 pC/N (41) for Li-substituted KNN prepared by similar methods.

3.4.2 Electromechanical coupling coefficients (k_p, k_t)

The electromechanical coupling coefficients obtained for each material composition are presented in Figure 3.14.

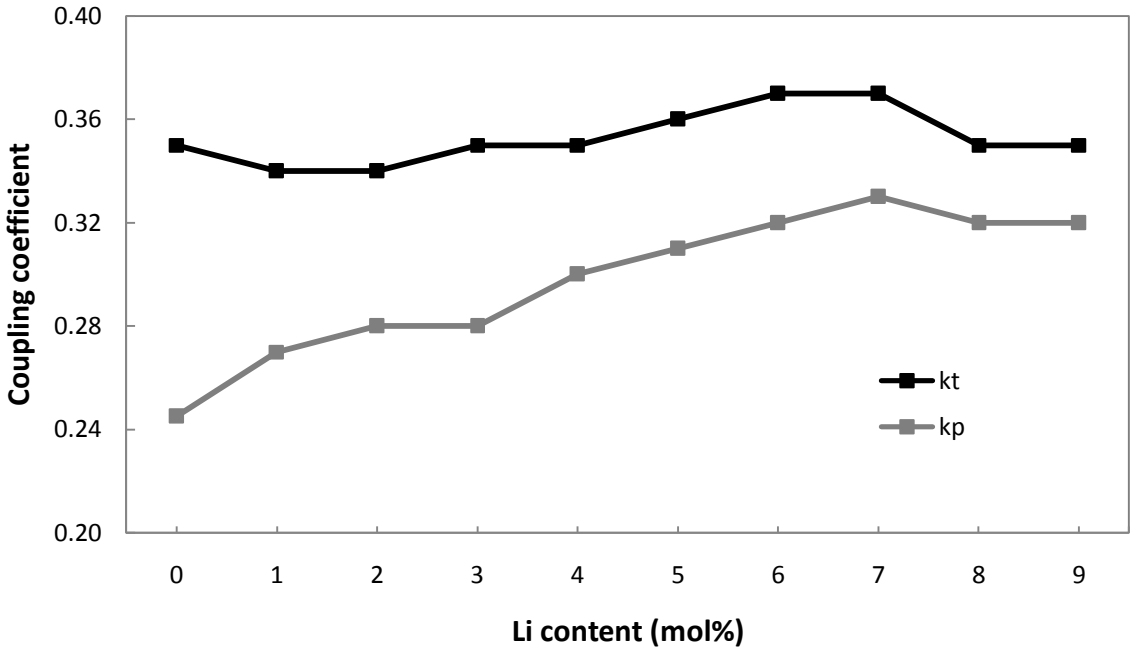

Figure 3.14 Electromechanical coupling coefficients (k_p, k_t) of Li-substituted KNN as a function of lithium content

Similar to the d_{33} results, both coupling coefficients peak at compositions near the O-T phase transition, with samples with a 7 mol% Li content exhibiting the highest performance in both instances, whilst increasing the lithium content further results in a decrease of properties. This therefore indicates that the composition $[(K_{0.5}Na_{0.5})_{0.93}Li_{0.07}]NbO_3$ has the highest sensitivity and is the most efficient material in converting electric energy into mechanical energy.

The k_p coefficient appears more sensitive to lithium content than the k_t coefficient, increasing 32% between samples of undoped KNN and those with 7 mol% Li content. Conversely, the k_t value increases by just 6% between the same two compositions with no

improvement observed until the lithium content is raised to 5 mol%. This disparity is consistent with other studies on Li-substituted KNN (20). With the (k_t/k_p) ratio lowered from 1.4 → 1.1 between 0-7 mol% Li, the result is a reduction in electromechanical anisotropy. This is often not a desirable consequence, as a high electromechanical anisotropy is useful in reducing cross talk between elements and reducing interference from higher harmonics in many piezoelectric transducer applications.

3.4.3 Relative permittivity (ε_r)

The relative permittivity was calculated at three separate frequencies for each material composition. The results are shown in Figure 3.15.

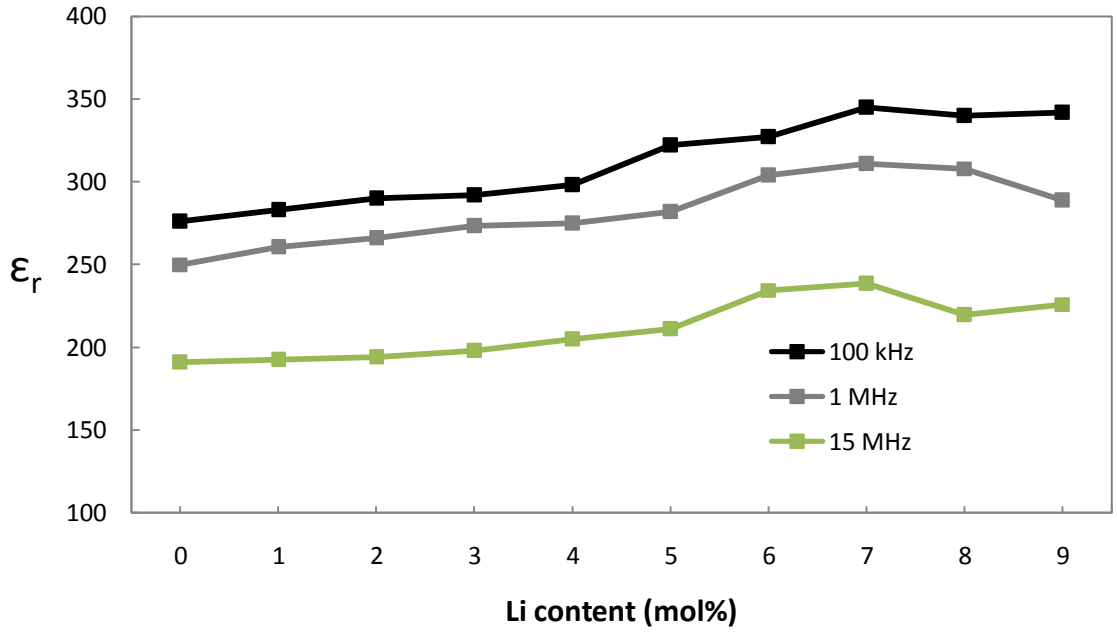

Figure 3.15 Relative permittivity for 3 separate frequencies as a function of lithium content

The relative permittivity (ε_r) values obtained for each composition follow a familiar pattern (Fig 3.15), increasing steadily with lithium content. The lowest values of ε_r are reported for the undoped KNN samples and highest values for samples with 7 mol% lithium content at

all three of the measured frequencies. The extent of the increase is very similar for all three frequencies. Between 0-7 mol% Li, permittivity increased by 25% at 100 kHz and 5 Mhz, and 24% at 1 Mhz. However, permittivity has not increased to the extent that would have been expected. As discussed in Chapter 1, there are reports of relative permittivity more than doubling between 4 mol% and 7 mol% Li content in KNN ceramics (23). Other studies have observed permittivity to be independent of lithium below a 4 mol% Li concentration, which is not the case in this study. The obtained values show strong frequency dependence, with relative permittivity deteriorating by ~40% between 100 kHz and 15 MHz for samples of the same composition. This gives an insight into how these materials might behave at high operating frequencies.

The complete set of functional properties obtained for $[(K_{0.5}Na_{0.5})_{1-x}Li_x]NbO_3$ are presented in Table 3.2.

Table 3.2 Piezoelectric properties of $[(K_{0.5}Na_{0.5})_{1-x}Li_x]NbO_3$ ceramics

Chemical composition	Density (g/cm^3)	Relative Density (%)	d_{33} (pC/N)	k_p	k_t	ε_r
$(K_{0.5}Na_{0.5})NbO_3$	3.85	85	114	0.25	0.35	239
$[(K_{0.5}Na_{0.5})_{0.99}Li_{0.01}]NbO_3$	3.85	85	112	0.27	0.34	245
$[(K_{0.5}Na_{0.5})_{0.98}Li_{0.02}]NbO_3$	3.88	86	113	0.28	0.34	250
$[(K_{0.5}Na_{0.5})_{0.97}Li_{0.03}]NbO_3$	3.91	87	112	0.28	0.35	255
$[(K_{0.5}Na_{0.5})_{0.96}Li_{0.04}]NbO_3$	3.93	87	115	0.30	0.35	259
$[(K_{0.5}Na_{0.5})_{0.95}Li_{0.05}]NbO_3$	3.99	88	120	0.31	0.36	272
$[(K_{0.5}Na_{0.5})_{0.94}Li_{0.06}]NbO_3$	4.08	90	121	0.32	0.37	289
$[(K_{0.5}Na_{0.5})_{0.93}Li_{0.07}]NbO_3$	4.14	92	126	0.33	0.37	298
$[(K_{0.5}Na_{0.5})_{0.92}Li_{0.08}]NbO_3$	4.07	90	126	0.32	0.35	289
$[(K_{0.5}Na_{0.5})_{0.91}Li_{0.09}]NbO_3$	4.08	90	124	0.32	0.35	286

When examining the relationship the functional properties have with density, many of the properties increase disproportionately to the density. The density itself increased by 8% between Li(x) concentrations of x=0 and x=0.07, whilst d_{33} increased by 11%, k_p by 32% and relative permittivity (ε_r) by 25%, with only k_t improving disproportionately less than the density (5.5%).

The crystal structure of the ceramic appears to be another influencing factor on the properties. According to XRD analysis, the orthorhombic to tetragonal phase transformation begins at x=0.04 and it is at Li concentrations in the compositional region $0.05<x<0.07$ where lithium has the greatest influence on properties and where optimum properties are achieved. As discussed in Chapter 1, optimum piezoelectric properties are often reported in this region. The structural instabilities induced in the material in the region of the O-T phase transition are thought to contribute to this. Samples with the orthorhombic crystal structure ($0.01<x<0.04$) still show improved ε_r and k_p values over undoped samples, but d_{33} and k_t do not benefit from lithium addition until higher concentrations.

Although samples were only fabricated up to a lithium content of x=0.09, the piezoelectric properties begin to show signs of degradation at $x>0.07$. Large quantities of the low density secondary phase identified by XRD analysis may be present, adversely affecting functional properties by lowering the density and reducing stoichiometry. Other research on Li-substituted KNN confirms that the piezoelectric properties continue to deteriorate past this point. Guo et al. fabricated KNN with up to 20 mol% Li content, and both density and piezoelectric properties were found to be lower than for undoped KNN (20).

Despite the enhanced properties achieved through the addition of lithium, the results are on the low side when compared to those achieved in other studies on Li-doped KNN. Whilst

the general trend is the same, with properties peaking around the O-T phase transition, some research has shown much larger improvements to the piezoelectric properties than what has been achieved in this study, most notably reports of ε_r and d_{33} almost doubling in the compositional range $0.05<x<0.07$ (20) (23). When speculating on why the properties fall short of literature values, there could be a variety of reasons. One of the key factors is likely to be the relatively poor sample densities obtained in this study compared to those reported in some published work. The functional properties measured have been shown to respond positively to an increase in density. It is therefore reasonable to assume that if higher densities comparable to those obtained in other literature had been achieved, improved functional properties would have been observed.

A loss of stoichiometry is another possibility. Near the phase boundary there is a strong compositional dependence. If the stoichiometry of the mixture was not exactly correct at the initial powder mixing stage, properties may have been adversely affected. However, any large discrepancies would have been identified by XRD.

Another factor to consider is the geometry of the samples used for the functional measurements. As described in Chapter 2, the samples characterised in this project were fabricated to give a geometry suited to thickness and radial modes of vibration for calculating the electromechanical coupling coefficients. Studies have found certain piezoelectric properties to be strongly dependant on sample aspect ratio. Barzegar et al. (42) have shown in their study investigating the effect of sample aspect ratio on d_{33} that measured d_{33} increases with increasing aspect ratio and reaches its true value at a threshold aspect ratio dependant on the ceramic composition. As the samples fabricated in this project feature a small aspect ratio (~0.05), increasing this would likely have yielded higher d_{33} measurements more comparable to what others have achieved. Another thing to

note is the slight variation in aspect ratio between samples. Whilst all samples were ground to a thickness of 0.5 mm, some sample compositions densified better than others and as such sample diameter varied depending on the level of shrinkage undergone in each sample, resulting in a slight variation in aspect ratio.

4. CONCLUSION

The piezoelectric ceramic potassium sodium niobate (KNN) chemically modified by lithium substitution has been investigated. Disc-shaped samples of $[(K_{0.5}Na_{0.5})_{1-x}Li_x]NbO_3$ (x=0-0.09) were successfully fabricated and their functional properties measured.

Lithium was found to aid with densification of the ceramic during sintering, with a maximum relative density of 92% achieved. SEM analysis confirmed that lithium had a noticeable influence on the microstructure of the sintered ceramics, promoting increased grain growth.

XRD analysis identified a transformation from the orthorhombic phase to the tetragonal phase with the introduction of lithium. Samples with the orthorhombic crystal structure (x<0.04) exhibited properties that were less responsive to lithium substitution compared to those in which the phase transformation was underway (x>0.04), but in both instances, the presence of lithium was beneficial in enhancing the piezoelectric properties to varying degrees.

Peak piezoelectric properties d_{33}=126 pC/N, k_p=0.33 and k_t=0.37 were obtained for samples of composition x=0.07. Chemical analysis of these samples indicates the tetragonal crystal structure is the dominant one, although it is unclear whether a complete transformation has occurred or not, with the likelihood being that both tetragonal and orthorhombic phases are in coexistence.

Despite the enhanced properties achieved through the addition of lithium to KNN, it still does not compare favourably with the market leader PZT, which continues to have the best properties for many piezoelectric-related applications. The potential is still there for KNN-based ceramics however. It responds well to dopants, does not contain lead and has a low

density. The densities achieved in this particular study are still some way below the theoretical density of KNN. If the relative density can be further improved by optimising the fabrication route, and research continues into establishing the most effective dopants, the functional properties of KNN can be further improved.

In conclusion, this project has shown that it is possible to fabricate functioning KNN samples by pressureless sintering, and that through the addition of lithium as a dopant material, the key piezoelectric properties can be improved.

5. FURTHER WORK

As one of the main stumbling blocks in the early stages of processing is the moisture sensitivity of K_2CO_3, different precursors for the alkali elements could be investigated. One that others have already had success with is sodium potassium tartrate tetrahydrate, a double salt of K and Na (43). This could make handling the pre-calcined powders easier. A higher temperature for the initial drying stage may also prove beneficial, as 100 °C may not be sufficient to fully dehydrate the alkali carbonates.

For thin, disc-shaped samples such as those fabricated in this project, a processing route that has proven successful in the fabrication of fine-scale PZT structures could be of interest. The viscous polymer processing technique (44) results in a high strength, de-agglomerated green-state material, and could be a possible alternative to the conventional powder pressed method used extensively for KNN.

KNN shows piezoelectric properties that are sensitive to processing. The effect of variables such as sintering time/heating rate and poling conditions could be investigated in more detail. Liu et al. has found heating rates to have a considerable effect on the density and thus the functional properties of Li-modified KNN ceramics (41). Optimum sintering conditions would likely vary for samples of different lithium content. In this project, a fixed sintering temperature was used (1100 °C), but in future studies, it would be beneficial to determine the ideal sintering temperature of each individual ceramic composition.

Given that optimum piezoelectric properties are found in compositions where the O-T phase transition temperature has been lowered to room temperature, question marks remain over the temperature stability of Li-modified ceramics. All functional

measurements in this study were carried out at room temperature, so further characterisation at varying temperatures would be beneficial in determining the extent to which properties are dependent on temperature.

For lithium doped KNN to fulfil its potential a clearer understanding of the $(K,Na)NbO_3$-$(Li)NbO_3$ phase diagram is needed. Through studying the phase transitions over a broad temperature range, Klein et al. have found the presence of a vertical MPB in Li-doped KNN at subzero temperatures (38). If this MPB could be raised into more practically used temperature ranges through chemical modification, then temperature independent properties could be achieved.

6. REFERENCES

1. **Ledbetter, H. Ogi, H. Nakamura, N.** Elastic, anelastic, piezoelectric coefficients of monocrystal lithium niobate. *Mechanics of Materials.* 2004, 36, pp. 941-947.

2. **Karaki, T. Yan, K. Adachi, M.** High-Performance Lead-free Barium Titanate Piezoelectric Ceramics. *Advances in Science and Technology.* 2008, Vol. 54, pp. 7-12.

3. **Takahashi, H. Numamato, Y. Tani, J. Matsuta, K. J, Qiu, Tsurekawa, S.** Lead-Free Barium Titanate Ceramics with Large Piezoelectric Constant Fabricated by Microwave Sintering. *Japanese Journal of Applied Physics.* 2006, Vol. 45, pp. L30-L32.

4. **Li, Y. Cheng, L. Gu, X. Zhang, Y. Liao, R.** Piezoelectric and dielectric properties of PbNb2O6-based piezoelectric ceramics with high Curie temperature. *Journal of Materials Processing Technology.* 2008, Vol. 197, pp. 170-173.

5. **Kakimoto, K. Yoshifuji, T. Ohsato, H.** Densification of tungsten-bronze KBa2Nb5O15 lead-free piezoceramics. *Journal of the European Ceramic Society.* 2007, Vol. 27, pp. 4111-4114.

6. **Jiang, W. Cao, W. Yi, X. Chen, H.** The elastic and piezoelectric properties of tungsten bronze ferroelectric crystals (Sr0.7Ba0.3)2NaNb5O15 and (Sr0.3Ba0.7)2NaNb5O15. *Journal of Applied Physics.* 2005, Vol. 97.

7. **Oliver, J. Neurgaonkar, R. Cross, L.** Ferroelectric Properties of Tungsten Bronze Morphotropic Phase Boundary Systems. *Journal of the American Ceramic Society.* 1989, Vol. 72, 2, pp. 202-211.

8. **Shebanov, L. Korzunova, L.** Perovskite-like compounds with bismuth layer structure: some new materials and phase transitions. *Mat. Res. Bull.* 1985, Vol. 20, pp. 781-786.

9. **Smolenskii, GA. Isupov VA. Agranovskaya, AI. Krainik, NN.** New ferroelectrics of complex compositions. *Sov. Phys. Solid State.* 1961, Vol. 2, 11, pp. 2651-2654.

10. **Panda, PK.** Review: environmental friendly lead-free piezoelectric materials. *J Mater Sci.* 2009, Vol. 44, pp. 5049-5062.

11. **Li, Y. Chen, W. Zhou, J. Xu, Q. Sun, H. Xu, R.** Dielectric and piezoelectric properties of lead-free (Na0.5Bi0.5)TiO3-NaNbO3 ceramics. *Materials Science and Engineering B.* 2004, Vol. 112, pp. 5-9.

12. **Chan, HLW. Choy, SH. Chong, CP. Li, HL. Liu, PCK.** Bismuth sodium titanate based lead-free ultrasonic transducer for microelectronics wirebonding applications. *Ceramics International.* 2008, Vol. 34, pp. 773-777.

13. **Ferroperm.** Ferroperm Materials programme. *Ferroperm Piezoceramics A/S.* [Online] http://ferroperm-piezo.com/.

14. **Berlincourt, D.** [book auth.] OE. Mattiat. *Ultrasonic Transducer Materials: Piezoelectric Crystals and Ceramics.* 1971, 2.

15. **Jaffe, H.** Piezoelectric Ceramics. *J. Am. Ceram. Soc.* 1958, Vol. 41, pp. 494-498.

16. **Yoo, J. Oh, D. Jeong, Y. Hong, J. Jung, M.** Dielectric and piezoelectric characteristicsof lead-free Bi0.5(Na0.84K0.16)0.5TiO3 ceramics substituted with Sr. *Materials Letters.* 2004, Vol. 58, pp. 3831-3835.

17. **Li, H. Feng, C. Yao, W.** Some effects of different additives on dielectric and piezoelectric properties of (Bi1/2Na1/2)TiO3-BaTiO3 morphotropic-phase-boundary composition. *Materials Letters.* 2004, Vol. 58, pp. 1194-1198.

18. **Takenaka, T. Maruyama, K. Sakata, K.** (Bi1/2Na1/2)TiO3-BaTiO3 System for Lead-Free Piezoelectric Ceramics. *Jpn. J. Appl. Phys.* 1991, Vol. 30, pp. 2236-2239.

19. **Jaeger, RE. Egerton, L.** Hot pressing of potassium-sodium niobates. *J. Am. Ceram. Soc.* 1962, Vol. 45, 5, pp. 209-213.

20. **Guo, Y. Kakimoto, K. Ohsato, H.** Phase transitional behavior and piezoelectric properties of (Na0.5K0.5)NbO3-LiNbO3 ceramics. *Applied Physics Letters.* Vol. 85, 18, pp. 4121-4123.

21. **Wang, R. Xie, R. Sekiya, T. Shimojo, Y.** Fabrication and characterisation of potassium-sodium niobate piezoelectric ceramics by spark-plasma-sintering method. *Materials Research Bulletin.* 2004, Vol. 39, pp. 1709-1715.

22. **Li, J. Wang, K.** Ferroelectric and Piezoelectric Properties of Fine-Grained Na0.5K0.5NbO3 Lead-Free Piezoelectric Ceramics Prepared by Spark Plasma Sintering. *J. Am. Ceram. Soc.* 2006, Vol. 89, 2, pp. 706-709.

23. **Hollenstein, E. Davis, M. Damjanovic, D. Setter, N.** Piezoelectric properties of Li- and Ta-modified (K0.5Na0.5)NbO3 ceramics. *Applied Physics Letters* . 2005, Vol. 87.

24. **Matsubara, M. Yamaguchi, T. Kikuta, K. Hirano, S.** Sinterability and Piezoelectric Properties of (K,Na)NbO3 Ceramics with Novel Sintering Aid. *Jpn. J. Appl. Phys.* 2004, Vol. 43, 10, pp. 7159-7163.

25. **Nakamura, K. Tokiwa, T. Kawamura, Y.** Domain structures in KNbO3 crystals and their piezoelectric properties. *Journal of Applied Physics.* 2002, Vol. 91, 11, pp. 9272-9276.

26. **Demartin Maeder, M. Damjanovic, D. Setter, N.** Lead Free Piezoelectric Materials. *Journal of Electroceramics.* 2004, 13, pp. 385-392.

27. **Egerton, L. Dillon, DM.** Piezoelectric and dielectric properties of ceramics in the system potassium-sodium-niobate. *J. Am. Ceram. Soc.* 1959, Vol. 42, 9, pp. 438-442.

28. **Feuillard, G. Loyau, V. Tran Huu Hue, L. Wurlitzer, T. Ringgaard, E. Wolny, W. Malic, B. Kosec, M. Barzegar, A. Damjanovic, D. Lethiecq, M.** Comparative performances of new KNN lead-free piezoelectric materials and classical lead-based ceramics for ultrasonic transducer applications. *2003 IEEE Ultrasonics Symposium.* 2003, pp. 1995-1998.

29. **Rodel, J. Jo, W. Seifert, K. Anton, E. Granzow, T.** Perspective on the Devlopment of Lead-free Piezoceramics. 2009, Vol. 92, 6, pp. 1153-1177.

30. **Du, H. Liu, D. Tang, F. Zhu, D. Zhou, W.** Microstructure, Piezoelectric, and Ferroelectric Properties of Bi2O3-Added (K0.5Na0.5)NbO3 Lead-Free Ceramics. *J. Am. Ceram. Soc.* 2007, Vol. 90, 9, pp. 2824-2829.

31. **Ringgaard, E. Wurlitzer, T.** Lead-free piezoceramics based on alkali niobates. *Journal of the European Ceramic Society.* 2005, Vol. 25, pp. 2701-2706.

32. **Egerton, L. Bieling, CA.** Isostatically hot-pressed sodium-potassium niobate transducer material for ultrasonic devices. *Ceram. Bull.* 1968, Vol. 47, 12, pp. 1151-1156.

33. **Saito, Y. Takao, H. Tani, T. Nonoyama, T. Takatori, K. Homma, T. Nagaya, T. Nakamura, M.** Lead-free piezoceramics. *Letters to Nature.* 2004, Vol. 432, pp. 84-87.

34. **Bernard, J. Bencan, A. Rojac, T. Holc, J. Malic, B. Kosec, M.** Low-Temperature Sintering of K0.5Na0.5NbO3 Ceramics. *J. Am. Ceram. Soc.* 2008, Vol. 91, 7, pp. 2409-2411.

35. **Zuo, R. Roedel, J. Chen, R. Li, L.** Sintering and electrical properties of lead-free Na0.5K0.5NbO3 piezoelectric ceramics. *J. Am. Ceram. Soc.* Vol. 89, pp. 2010-2015.

36. **Zhang, S. Xia, R. Shrout, T.** Modified (K0.5Na0.5)NbO3 based lead-free piezoelectrics with broad temperature usage range. *Applied Physics Letters.* 2007, Vol. 91.

37. **Sun, Y. Xiao, D. Wu, L. Lin, D. Zhu, J. Yu, P. Li, X. Wang, Y. Li, Y. Lin, Y. Zhuang, Y. Wei, Q.** Microstructure and properties of lithium and antimony modified potassium sodium niobate lead-free piezoelectric ceramics. *Journal of the Ceramic Society of Japan.* 2008, Vol. 116, 4, pp. 536-539.

38. **Klein, N. Hollenstein, E. Damjanovic, D. Trodahl, H. Setter, N.** A study of the phase diagram of (K,Na,Li)NbO3 determined by dielectric and piezoelectric measurements, and Raman spectroscopy. *Journal of Applied Physics.* 2007, Vol. 102.

39. **Du, H. Zhou, W. Luo, F. Zhu, D. Qu, S. Li, Y. Pei, Z.** Structure and electrical properties' investigation of (K0.5Na0.5)NbO3-(Bi0.5Na0.5)TiO3 lead-free piezoelectric ceramics. *J. Phys. D: Appl. Phys.* 2008, Vol. 41.

40. **Sen, C. Alkan, B. Akin, I. Yucel, O. Sahin, F. Goller, G.** Microstructure and ferroelectric properties of spark plasma sintered Li substituted K0.5Na0.5NbO3 ceramics. *Journal of the Ceramic Society of Japan.* 2011, Vol. 119, 5, pp. 355-361.

41. **Liu, D. Du, H. Tang, F. Luo, F. Zhu, D. Zhou, W.** Effect of heating rate on the structure evolution of (K0.5Na0.5)NbO3-LiNbO3 lead-free piezoelectric ceramics. *J Electroceram.* 2008, Vol. 20, pp. 107-111.

42. **Barzegar, A. Damjanovic, D. Setter, N.** The effect of boundary conditions and sample aspect ratio on apparent d33 piezoelectric coefficient determined by direct quasistatic method. *IEEE Trans. Ultrason. Ferroelect. Freq. Contr.* 2004, Vol. 51, 3, pp. 262-269.

43. **Malic, B. Bernard, J. Holc, J. Jenko, D. Kosec, M.** Alkaline-earth doping in (K,Na)NbO3 based piezoceramics. *Electroceramics.* 2005, Vol. 4, pp. 2707-2711.

44. **Abrar, A. Zhang, D. Su, B. Button, T. Kirk, K. Cochran, S.** 1-3 connectivity piezoelectric ceramic-polymer composite transducers made with viscous polymer processing for high frequency ultrasound. *Ultrasonics.* 2004, Vol. 42, pp. 479-484.